



Buffeting performance of long-span bridges with different span affected by parametric typhoon wind

Lin Zhao ^{a,b,c,d}, Zilong Wang ^a, Weile Chen ^e, Wei Cui ^{a,b,*}

^a State Key Lab of Disaster Reduction in Civil Engineering, Tongji University, Shanghai, 200092, China

^b Key Laboratory of Transport Industry of Wind Resistant Technology for Bridge Structures (Tongji University), Shanghai, 200092, China

^c College of Civil Engineering and Architecture, Guangxi University, Nanning, 530004, China

^d Key Laboratory of Disaster Prevention and Structural Safety of China Ministry of Education, Guangxi University, Nanning, 530004, China

^e Guangdong Provincial Highway Construction Company Limited, Guangzhou, 510000, China

ARTICLE INFO

Keywords:

Long-span bridge
Typhoon process
Parametric wind field
Buffeting performance
Wind tunnel test

ABSTRACT

Currently, typhoon-related performance of long span bridges usually focus on a specific wind record such as wind speed and turbulence intensity during a full typhoon, however, the inter-correlation among wind characteristic parameters under typhoon wind climate is ignored. The existing investigation about structural responses during typhoon attacks are still limited at case-study analysis, and hardly provide a generalized framework to evaluate the structural performance especially for typhoon landing whole process. This study utilizes the measured wind speeds of the strong typhoon "Hagupit" to establish a unified typhoon parametric model, during which the correlation of typhoon wind parameters including angle of attack (AoA), turbulence intensity, integral length scale and mean wind speed were taken into consideration. The measured typhoon process characterized with center-through effect with M-type average wind speed curve. Furthermore, the structural performance of long-span bridges with different spans from 1500 m to 2500 m main span was systematically studied. The aerodynamic parameters of the bridge deck section, including the aerostatic coefficients, flutter derivatives at different AoAs, and aerodynamic admittance under different oncoming flow conditions were identified through wind tunnel tests. Finally, the wind-induced buffeting performance was calculated by the buffeting frequency domain algorithm, showing various structural wind effect characteristics during the typhoon landing whole process. The maximal buffeting response is not necessarily related with the wind speed, and other wind characteristics especially turbulence intensity and AoA, etc. also affect on the results.

1. Introduction

Bridge spans have been rapidly increasing due to advanced construction techniques and huge society development requirement, up to now, the main span of Çanakkale Bridge in Turkey exceeded 2000 m as the largest span bridge in 2021. As main span has been gradually developing, the stiffness and damping ratio of the bridge structures gradually decrease, causing the bridge structures become more vulnerable to wind-induced vibration. On the other hand, long-span bridges normally were employed to cross the sea strait in typhoon-prone areas. Besides higher wind speeds, typhoons wind environment with more severe characteristics than those of the synoptic monsoon climate, such as angle of attack (AoA), high turbulence intensity, and irregular wind spectrum. All of these lead to the complex performance of buffeting

response of long-span bridges under typhoon state. Buffeting with large amplitude vibration severely threats the bridge structural safety and comfort of vehicles driving, and the buffeting response for long-span bridges evaluation considering the complex non-synoptic wind field parameters should be paid more attention to the safety construction and operation (Ge and Zhao, 2014).

The preliminary research on typhoons mainly emphasized on the intensity level of typhoons, and then many scholars have carried out related research on the typhoon wind field and characteristics of wind turbulence. According to the measured data of the typhoon by Liu et al. (2021), larger wind AoAs caused by the updraft especially near the typhoon eye, and the turbulence intensity in typhoon wind field is significantly higher than that of the synoptic wind, and it characters with different wind spectrum function before and after landfall (Ishizaki,

* Corresponding author. State Key Lab of Disaster Reduction in Civil Engineering, Tongji University, Shanghai 200092, China.

E-mail address: cuiwei@tongji.edu.cn (W. Cui).

1983), (Cao et al., 2009; Li et al., 2010; Tamura et al., 1993). By comparing the radius of maximum wind speed and radial pressure distribution of measured typhoon data, various typhoon models and associated field parameters for different ocean region have been proposed by Fang et al. (2021). The correlation between various typhoon field parameters has also been quantitatively analyzed based on health monitoring data by Zhao et al. (2019).

According to the wind loading chain of Davenport (Isyumov and Alan, 2012), the analysis of buffeting response needs to combine wind climate, aerodynamics in fluid-structure interaction and structural dynamics. The bridge buffeting algorithm was firstly derived from the aerodynamic model of airfoil. Sears (1941) derived the formulas of the buffeting lift and torque of the thin airfoil model based on the potential flow theory, and proposed the concept of the aerodynamic admittance function. Liepmann (1952) combined the concept of probability and statistics in mathematics with the buffeting response of the wing model. Therefore, Davenport (1962) proposed the buffeting calculation method for bridge structure based on quasi-steady theory. The aerodynamic admittance function reflects the transfer function from the wind spectrum to the buffeting force spectrum, which was emphasize by but Davenport's theory, then, Scanlan et al. (1974, 1996, 2001) improved the method by considering the self-excited force. Scanlan and Davenport laid the foundation for the framework of buffeting theory. On their basis, Lin et al. (1993) proposed a linear time domain buffeting force model by using impulse response function. Then, Katsuchi et al. (1999) considered the changes of aerodynamic parameters with the axial direction of the bridge and conducted the flutter analysis on the Akashi Kaikyo Bridge. Furthermore, Seo et al. (2012) used the Monte-Carlo method to predict the buffeting response of long-span bridges, and gave the response vulnerability curves and surfaces. Bucher et al. (1988, 1990) proposed to use a unit impulse response function to represent the self-excited force, which can make it easier to find an expression form to describe the coupled aerodynamic force. Besides, Cui et al. (2021) (Zhang et al., 2023; Lei et al., 2023) also considered non-Gaussian effects of turbulence. Yi et al. (2022) summarized the changes in wind characteristics during typhoon landing, and summarized the changes in mean wind and turbulence intensity. Wang et al. (2009) and Fenerci et al. (2018) calculated the buffeting response of the bridge based on the measured typhoon data and considering the characteristics of the typhoon's large turbulence intensity. With the development of high-frequency wind field monitoring systems, the non-Gaussian nature of wind turbulence has become another factor of increasing concern in modern wind vibration analysis (Li et al., 2015). Hui et al. (2017) document non-Gaussian nature of wind fields. Cui et al. (2021, 2022) proposed a new calculation method for buffeting response of long-span bridges considering the non-Gaussian characteristics of typhoons. It was revealed that the typhoon field near the eye wall be of not only stronger wind velocity, but also non-stationary effect with time-varying coherence function (Xu et al., 2014). It is essential for nonstationary buffeting analysis of long-span bridges under typhoons (Hu et al., 2013; Tao et al., 2020). For this purpose, Huang et al. (2021) simulated a time-varying non-stationary typhoon and compared it with the measured values.

Most existing studies use measured data from typhoons to analyze turbulence-related characteristics. When processing typhoon wind parameters, most studies focus on analyzing the randomness and correlation of turbulence parameters. The probabilistic dependency among various wind field parameters and the wind-induced behavior of long-span bridges is relatively lacking, and it is difficult to conduct a unified study on the evolution of wind parameters during the entire typhoon process. In fact, there is the probabilistic dependence between wind parameters at different stages of a typhoon, and the turbulence characteristics can be associated with average wind speed. Therefore, it is necessary to propose a general framework that typhoon characteristics such as large AoA and strong turbulence-related parameters and its influence on the evaluate structural performance of long-span bridges. It would provide a reasonable reference for the wind resistance design of

wind sensitive. Thus, this study summarizes the variation of wind characteristics using field measured data before and after typhoon landfall, and covers the AoA, turbulence intensity, integral scale and the average wind speed to establish a unified typhoon effect evaluation model. For this purpose, the aerodynamic parametric of typical bridge sections were identified through forced vibration wind tunnel tests under the measured typhoon environment. Considering the multi-mode effect and aerodynamic coupling effect, the buffeting response of the target bridge was predicted through the three-dimensional buffeting frequency domain algorithm, then the evolution trend of the buffeting response of bridges with different spans under the typhoon process was summarized. Finally, the typhoon performance estimation framework is proposed to calculate the typhoon related dynamic performance of long-span bridges, providing a basis for wind resistance design and evaluation of long-span bridges.

2. Wind field parameters during typhoon landfall

The severe typhoon "Hagupit" (0814) was formed in the northwestern Pacific east of the Philippines on September 15, 2008 and upgraded to a tropical depression on September 17. Its intensity evaluation process is shown in Fig. 1. The typhoon observation tower was located on Zhizai Island. The height of the observation tower is 100 m. Zhizai Island is an uninhabitable island with a distance of 4.5 km from the mainland of China. The landing path of typhoon "Hagupit" and the location of the observation station are shown in Fig. 1. The observation was recorded with three-dimensional ultrasonic anemometers which were fixed at a height of 60 m on the observation tower. The sampling frequency is 10 Hz. The resolution is ± 0.01 m/s, the accuracy is 1.5% RMS and the measuring range is 0–65 m/s.

2.1. Typhoon field characteristics

The recorded "Hagupit" data is the three-directional instantaneous wind speed $u_x(t)$, $u_y(t)$, $u_z(t)$, in which x , y indicate horizontal wind velocity and z is vertical wind velocity. The time when the typhoon center passes the measuring station is T_0 , and the data of 12 h before and after passing the measuring station were recorded. The recording duration is 24 h from 6:00 p.m. on September 23 to 6:00 p.m. on September 24, 2008. The whole recording was divided into 144 groups with 10-min time interval. The average wind speed U and the yawing angle φ within the 10-min time interval are determined according to Eq. (1):

$$\begin{cases} U = \sqrt{\bar{u}_x(t)^2 + \bar{u}_y(t)^2} \\ \cos \varphi = \bar{u}_x(t)/U \end{cases} \quad (1)$$

where $\bar{u}_x(t)$ and $\bar{u}_y(t)$ represent the time variant averaged horizontal wind speed in the 10-min time interval. The time-history calculation formulas of the along-wind pulsating wind speed $u(t)$, the crosswind wind speed $v(t)$ and the vertical wind speed $w(t)$ are determined according to Eq. (2):

$$\begin{cases} u(t) = u_x(t)\cos \varphi + u_y(t)\sin \varphi - U \\ v(t) = -u_x(t)\sin \varphi + u_y(t)\cos \varphi \\ w(t) = u_z(t) \end{cases} \quad (2)$$

The wind AoA α is:

$$\alpha(t) = \arctan\left(\frac{\bar{w}(t)}{U}\right) \quad (3)$$

The turbulence intensity is defined as the ratio of the turbulence standard deviation to the average wind speed:

$$I_i = \frac{\sigma_i}{U}, i = u, v, w \quad (4)$$

where σ_i represents the standard deviation of the fluctuating wind speed

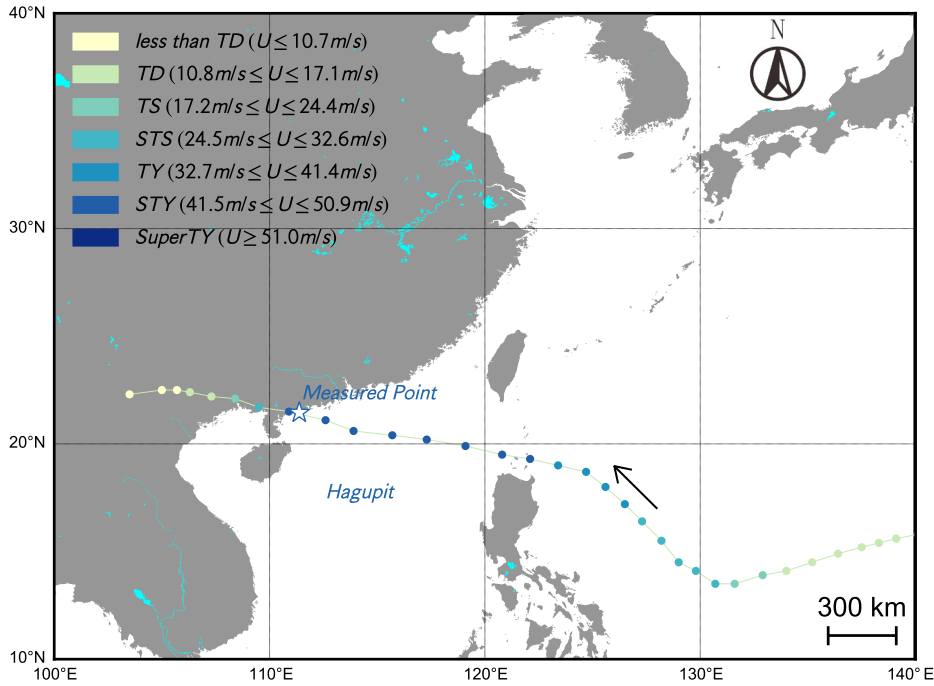


Fig. 1. Moving path of typhoon "Hagupit" (0814).

within 10-min of the average time interval in the i direction. The turbulence integral scale is the average size of the various vortices in the airflow along a specified direction. Mathematically, the turbulence integral scale is expressed:

$$L_i = \frac{1}{\sigma_i^2} \int_0^\infty C_{i_1 i_2}(r) dr \quad (5)$$

where $i = u, v, w$; $r = x, y, z$; σ_i^2 is the variance of the turbulence component i , C is the cross-covariance function between the turbulence at two spatial points separated by r . However, the calculation of the above formula must measure the fluctuating wind speed synchronously in a large enough space and at enough points, which is difficult to achieve in practice. In practical applications, the autocovariance function is replaced by the autocorrelation function, assuming that the vortices in the turbulent flow are transported downward without attenuation (Taylor's "vortex frozen transport" assumption). And the turbulence scale is defined as:

$$L_i^x = \frac{\bar{U}}{\sigma_i^2} \int_0^\infty R_j(\tau) d\tau, i = u, v, w \quad (6)$$

where \bar{U} is mean wind speed; σ_i^2 is the variance of corresponding pulsating wind speed; $R_j(\tau)$ is the auto-covariance of each velocity component. In this study, in order to get a consistent estimation of the integral scale, the autocorrelation function $R_j(\tau)$ is integrated numerically from $\tau = 0$ to the first crossing of $R_j(\tau) = 0$. And it is adopted to calculate the integral scale of the measured "Hagupit" data. In 1948, von Kármán (1948) proposed a theoretical model of fluctuating wind speed for u, v, w directions, respectively.

$$\frac{n \cdot S_u(n)}{\sigma_u^2} = \frac{4 \cdot \frac{nL_u}{U}}{\left[1 + 70.8 \cdot \left(\frac{nL_u}{U} \right)^2 \right]^{5/6}} \quad (7)$$

$$\frac{n \cdot S_v(n)}{\sigma_v^2} = \frac{4 \cdot \frac{nL_v}{U}}{\left[1 + 755 \cdot \left(\frac{nL_v}{U} \right)^2 \right]^{11/6}} \quad (8)$$

where n is the frequency; $S_u(n)$, $S_v(n)$, and $S_w(n)$ are the longitudinal, lateral, and vertical power spectrum of turbulence; L_u , L_v , and L_w are the longitudinal, lateral, and vertical turbulent integral scales; σ_u , σ_v , and σ_w are the standard deviations of the longitudinal, lateral, and vertical components of the fluctuating wind speed.

The fluctuating wind speed power spectra under typhoon environment are generally in good agreement with the von Kármán spectrum in the low frequency range. Therefore, the buffeting response calculation of long-span bridges was carried out based on the assumption of the von Kármán spectrum, since the frequencies of the front order mode shapes of long-span bridges are mostly concentrated in the low frequency region. The fitted von Kármán spectrum were employed to evaluate the bridge buffeting when simulating the pulsating wind velocity time history. Figs. 2 and 3 show the pulsating wind speed spectra in three directions in a measurement period before and after the center of "Hagupit" passes through the measuring station (T_0). The points before and after T_0 are No.46 and No.92 time series, respectively (shown in Fig. 4). And the wind characteristics of No.46 and No.92 are shown in Table 1.

According to Eqs. (1)–(6), the wind characteristic parameters of the typhoon are processed, and the results are shown in Fig. 4. The intensity of "Hagupit" changed from strong to weak after landfall, and the distance changed from near to far. Among them, the minimum distance from the typhoon center to the observation tower is about 10.0 km and the maximum one is 337.3 km. This range makes the observation tower always located in the strong influence area during typhoon process.

The average horizontal wind speed of "Hagupit" typhoon is in the range of 5–45.8 m/s, the highest 10-min time interval wind speed is close to 46 m/s, and the wind speed time history presents an M-shaped bimodal distribution. The wind speed at the top of the M peak reaches 46 m/s, the bottom reaches 11 m/s, and the wind speed difference is 35 m/s. At the same time, the wind direction before and after the landing of

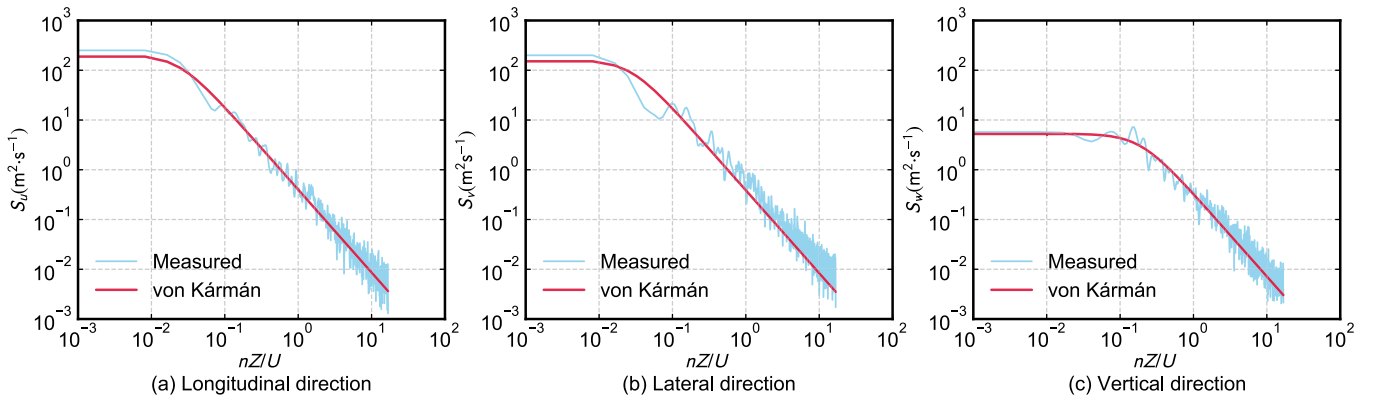


Fig. 2. No.46 wind speed spectra in three directions of typhoon “Hagupit”.

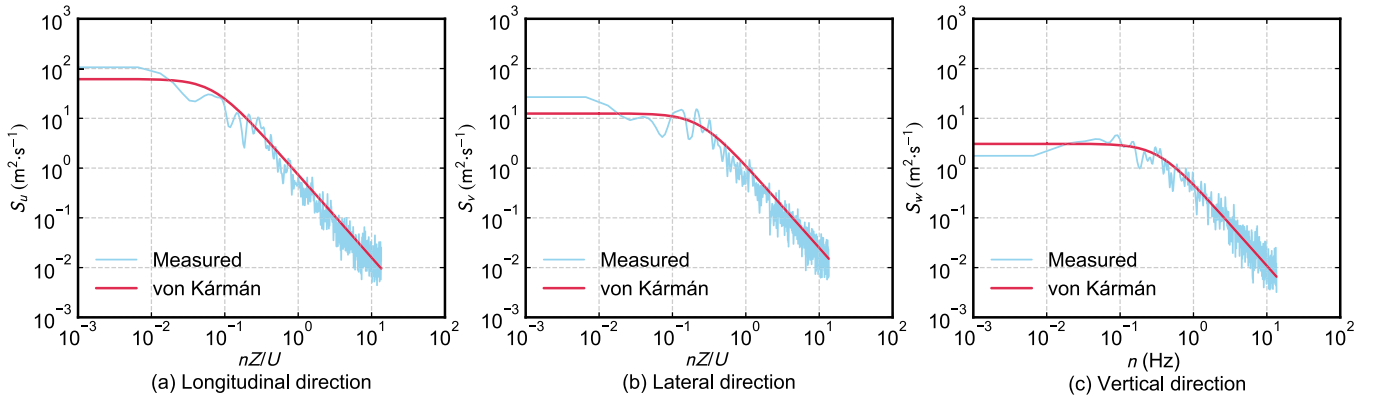


Fig. 3. No.92 wind speed spectra in three directions of typhoon “Hagupit”.

“Hagupit” experienced a conversion of nearly 180°, indicating that the observation of “Hagupit” experienced the typhoon eye. The measured wind AoAs range from -0.74° to 6.6°. The large AoA has an impact on aerodynamic parameters such as flutter derivatives, etc. Therefore, the wind characteristic parameters under strong typhoon conditions would be the key factors for bridge wind resistance safety design. And it can be seen from Fig. 4 that the along-wind, crosswind and vertical turbulence changes drastically before typhoon landfall, and the turbulence is relatively stable after landfall. After a long period of time after typhoons landed, there was a sudden increase in turbulence intensity, this phenomenon may be due to the disturbance for atmospheric circulation.

2.2. The unified parametric typhoon field

Most of the “Hagupit” wind field parameters are concentrated in the range of low wind speed, 2° AoA and low turbulence intensity. The wind speed time series turbulence character with higher wind speed, and larger AoA before and after the typhoon landfall have a predominant impact on the buffet performance of the bridges, which should be paid more attention. Therefore, in order to find the relationship between various parameters more clearly, and explore the relationship between various parameters, so-called a “typhoon field experienced regression parametric model (ERPM)” is finally proposed.

2.2.1. Wind speed and turbulence intensity

The turbulence intensity after the “M” first peak first decreases with the increase of wind speed, and when passing through the bottom of the M peak, the turbulence intensity increases with the decrease of wind speed. Turbulence intensity coupled with higher wind speeds has obviously influence on bridge buffeting response. Zhao et al. (2019) normalized the typhoon wind speed characteristics realizing

approximate dimensionless treatment by introducing the influence of spatial location and central deficit, etc., and obtained the relationship between the turbulence intensity and the reduced wind speed. Similar processing methods is adopted to explore the relationship between wind speed and turbulence intensity. The wind speed U_{max} of the “Hagupit” given by the meteorological station can be obtained. Define the average wind speed U_0 for a 10-min interval as:

$$U_0 = \sqrt{\overline{U_u}^2 + \overline{U_v}^2 + \overline{U_w}^2} \quad (9)$$

where $\overline{U_i}$ ($i = u, v, w$) represents the average wind speed in the longitudinal, lateral and vertical directions, respectively.

After the ratio of the measured average wind speed U_0 to the wind speed U_{max} at the corresponding time of the meteorological station (the dimensionless value of wind speed), the relationship between dimensionless wind speed and the turbulence intensity is shown in Fig. 5. Only high wind speed ($U_0 \geq 20$ m/s) is considered.

The blue dots in the figure represent the measured data before landing time T_0 , and the orange dots represent the measured data after T_0 . It can be found that the turbulence intensity of the “Hagupit” after landing increases with the increase of the reduced value of wind speed. With the increase of the reduced wind speed, the turbulence intensity before landing showed a trend of first decreasing and then increasing. From the results, the relationship model between wind speed and turbulence intensity can be approximately presented as:

$$I_u = k \cdot U_p + b \quad (10)$$

where, U_p is the ratio of the measured average wind speed at the 10-min measuring point to the maximum value of the typhoon meteorological data, k and b are fitting parameters, and I_u is the longitudinal turbulence

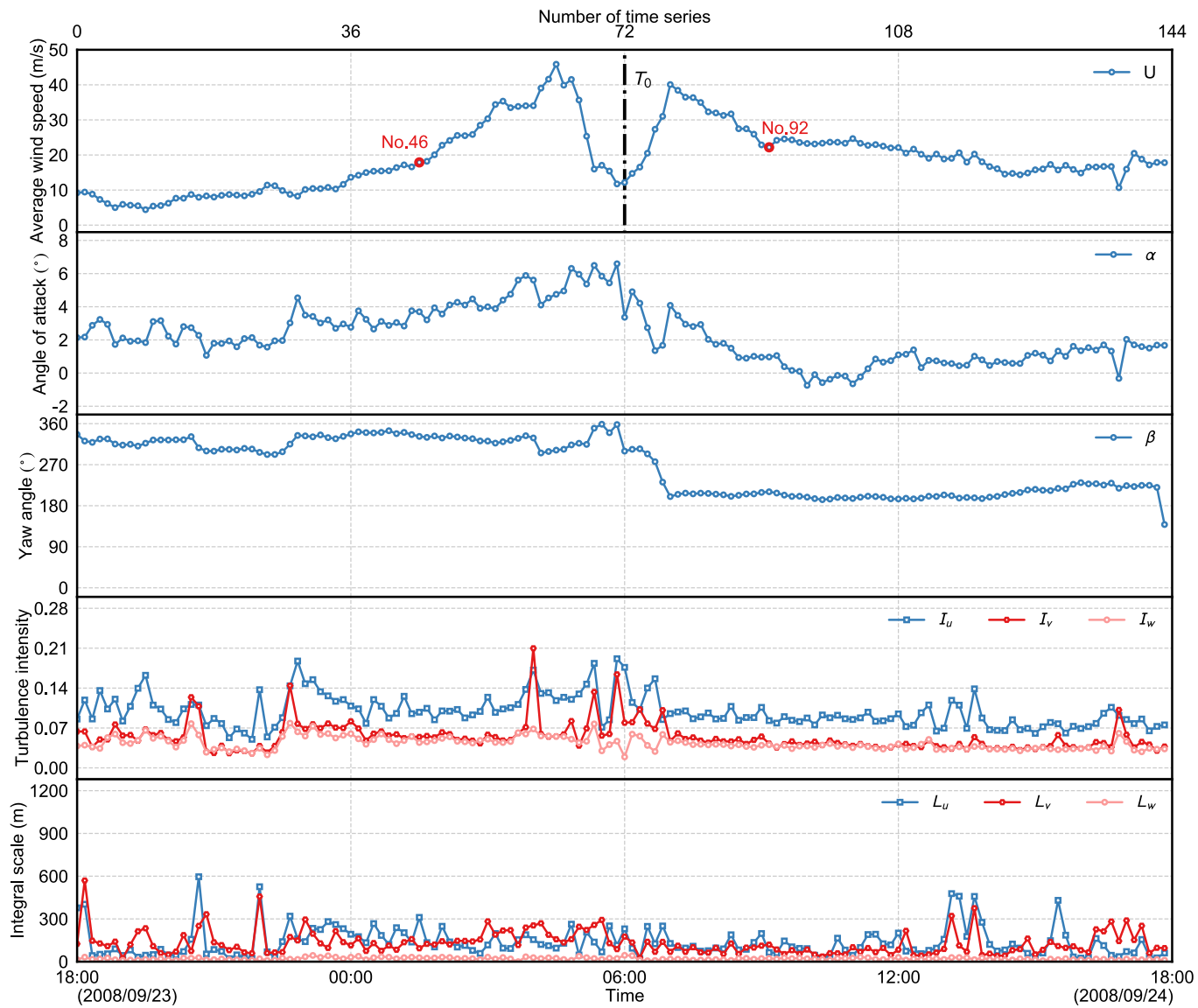


Fig. 4. Wind characteristics evolution of typhoon “Hagupit” (0814).

Table 1
Wind characteristics of No.46 and No.92 of typhoon “Hagupit” (0814).

Wind characteristics	U	I_u	I_v	I_w	L_u	L_v	L_w
No.46	17.89	0.0977	0.0542	0.0445	310.8181	94.0751	28.0072
No.92	22.19	0.0830	0.0426	0.0406	64.23657	119.4943	23.4336

intensity. The fitting values for the turbulence intensity of the “Hagupit” are shown in Table 2.

Similarly, the relationship between I_v and I_w is related to I_u , and they can be linearly fitted using Eq. (11). Table 3 and Fig. 6 give the fitting curve and observed results.

$$I_i = k \cdot I_u + b (i = v, w) \quad (11)$$

2.2.2. Wind speed and AoA

The time-history curve of wind speed and wind AoA is given as shown in Fig. 7. The maximum AoA at high wind speeds reached 6.6°. And the wind speed and wind AoA can be divided into 5 intervals.

- (1) Before the “Hagupit” Center passes the station time T_0 , the I_a and I_{a1} intervals are divided with a wind speed of 20 m/s;

- (2) The typhoon eye area of typhoon “Hagupit” across the center is divided into two parts, the highest wind speed to the lowest wind speed is the III_a zone, and the lowest to the highest wind speed is the III_b zone;
- (3) After T_0 , divide the II_b interval and the I_b interval with the wind speed of 20 m/s.

It can be found that the interval between I_a and I_b is the unstable area of the wind AoA, the wind speed is small, and the wind AoA fluctuates significantly. Areas II_a and II_b are the rapid rising and falling sections of wind speed and AoA before and after T_0 . At this time, it is found seen that there is a clear probabilistic correlation between wind speed and AoA. The rising rate of the wind AoA in area II_a is lower than that of the wind speed, and the decay rate of the wind AoA in area II_b is higher than

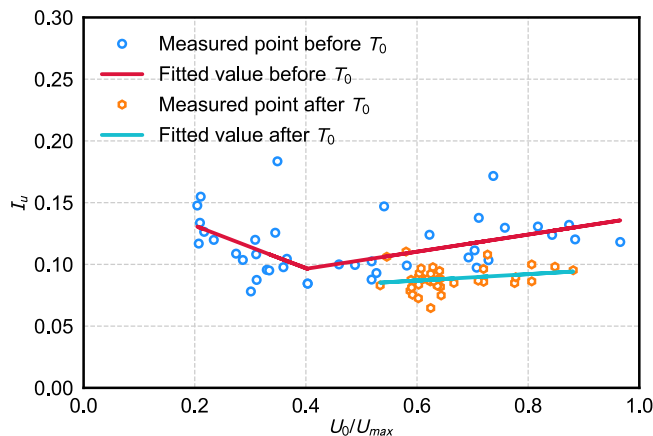


Fig. 5. Fitting curve of I_u and reduced value of wind speed.

Table 2
Fitting parameters between wind speed and turbulence intensity.

Parameter value	k	95% confidence interval	b	95% confidence interval
Before T_0 ($U_0/U_{max} < 0.4$)	-0.1727	[-0.3690, 0.0237]	0.1659	[0.1072, 0.2246]
Before T_0 ($U_0/U_{max} > 0.4$)	0.0693	[0.0121, 0.1265]	0.0687	[0.0293, 0.1080]
After T_0	0.0259	[-0.1223, 0.0639]	0.0714	[0.0461, 0.0966]

Table 3
Fitting parameters of turbulence intensities in three directions.

Parameter value	k	95% confidence interval	b	95% confidence interval
I_u	0.5638	[0.4521, 0.6754]	-0.0023	[-0.0137, 0.0091]
I_w	0.2634	[0.2090, 0.3177]	0.0171	[0.0116, 0.0227]

that of the wind speed, and at this time the wind AoA drops to the range of negative AoA. Areas III_a and III_b just lie in the typhoon eye areas. The change of the AoA in the eye area of typhoon can be divided into two parts: (1) From the highest point of wind speed to the lowest point of wind speed before T_0 , the AoA of wind still remains at the large attack point; (2) From the lowest point to the highest point of wind speed in the typhoon eye area, the wind AoA has an inverse relationship with the wind speed, and when the wind speed rises, the AoA also decreases

rapidly.

There are the low wind speed and large fluctuation of the AoA in the I_a and I_b intervals as shown in Fig. 8. And there is an obvious linear relationship between the wind AoA and wind speed in other areas. The fitting curves in Fig. 8 belong to a linear expression and the fitting parameters are given in Table 4.

2.2.3. Turbulence intensity and integral scale

Fig. 9 shows that there is an approximate linear relationship between turbulence intensity and integral scale. The turbulence integral scale increases with the increase of turbulence intensity.

By exploring the relationship between various wind characteristic parameters, the AoA and turbulence intensity are related to the wind speed, and the integral scale is related to the turbulence intensity, meaning that all parameters are probabilistic depend on the oncoming wind speed, and finally establishing a normalized wind characteristic chain. The parametric model can better analyze the influence of the combination of strong typhoon characteristic parameters for revealing the most unfavorable wind environment combination on the bridge structural performance.

The empirical regression parametric model through the measured typhoon process is shown in Fig. 10. Subsequently, the aerodynamic parameters identified by the wind tunnel test will be used to perform multi-modal buffeting calculations on long-span bridges, and the structural effect design envelope map will be further proposed.

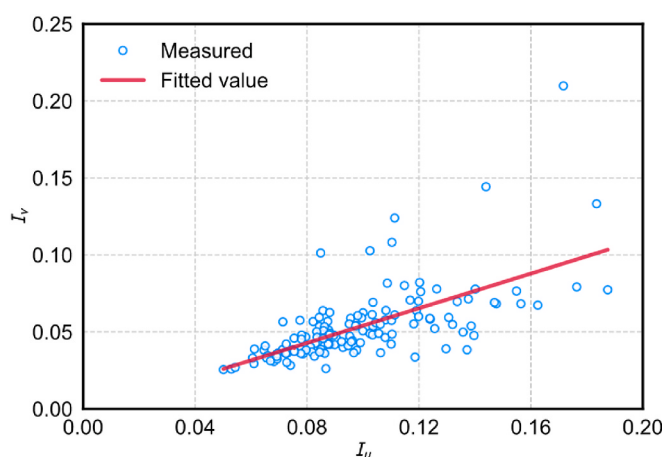
3. Aerodynamic parameters of bridge girder

3.1. Wind tunnel test

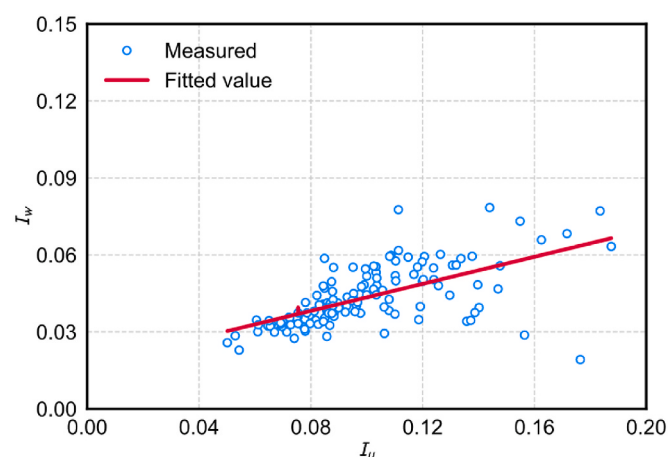
Furthermore, the aerodynamic parameters of the bridge that need to be used for structural analysis are obtained in the TJ-7 wind tunnel. The design wind speed of TJ-7 wind tunnel of Tongji University is 0–15 m/s. The wind tunnel test section is shown in Fig. 11. The cross-sectional size is 0.65 m × 1.2 m × 3.2 m, the maximum along-wind turbulence intensity is less than 2%, and the oncoming flow field stability is good, which is enough to conduct subsequent wind tunnel experiments. The related aerodynamic parameters were identified using the forced vibration device (Zhao et al., 2020).

The forced vibration device of Tongji University is driven by a pair of linear motors and controlled by a micron-scale grating. By inputting time-history signals, the forced vibration device can simulate various vibration modes (Zhao et al., 2020), including 3DoF motion modes as shown in Fig. 12.

Streamlined box girder sections are widely used in long-span bridges,



(a) The fitting relationship between I_u and I_v



(b) The fitting relationship between I_u and I_w

Fig. 6. Relationship between turbulence intensities in three directions.

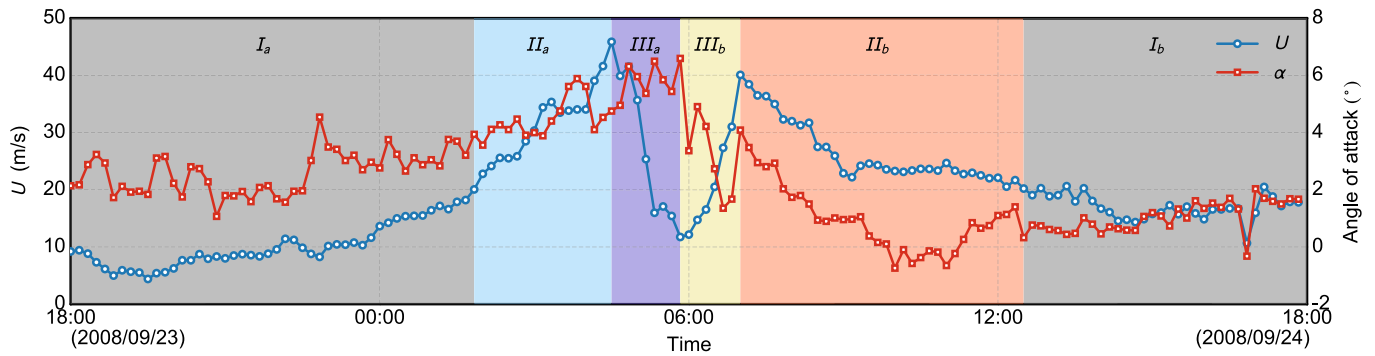


Fig. 7. Time history of wind speed and AoA.

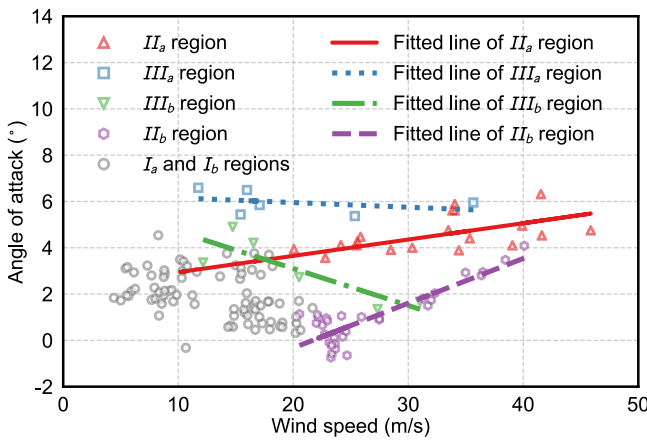


Fig. 8. Fitting curves of AoA and wind speed.

Table 4
Fitting curve parameters about AoA and wind speed.

Regions	II _a region	II _b region	III _a region	III _b region
<i>k</i>	0.0706	0.1933	-0.0200	-0.1590
<i>b</i>	2.2367	-4.1932	6.3570	6.2590

and there are auxiliary facilities such as railings and maintenance tracks. The model section dimensions are shown in Figs. 13 and 14. The width of the bridge segment model is 250 mm, the height is 21 mm, and the length of the segment model is 600 mm. In order to reduce the end effect of the model, two compensatory plates are added at the end of model, and the installation diagram of the model is shown in Fig. 15. Fig. 16

gives the definition of each force direction.

In the figure, D , L , M are lift, drag, torque, respectively, and θ is the AoA with positive definition counterclockwise.

3.2. Aerostatic coefficients

The average wind load experienced by the structure is called the static wind load. Under orthogonal oncoming wind, the drag, lift and torque coefficients under the wind axis coordinate are defined as:

$$C_D = \frac{F_D}{\frac{1}{2} \rho U^2 H}, C_L = \frac{F_L}{\frac{1}{2} \rho U^2 B}, C_M = \frac{M}{\frac{1}{2} \rho U^2 B^2} \quad (12)$$

where U is the wind speed, ρ is the air density, H and B are the height and width of the deck, respectively, F_D , F_L , M are the drag, lift and torque in the wind axis coordinate. The results of the aerodynamic coefficients and its derivative under the wind axis are shown in Fig. 17.

3.3. Flutter derivatives

The self-excited aerodynamic forces experienced by the structure can be expressed as a function related to the motion:

$$\begin{bmatrix} L \\ M \end{bmatrix} = \begin{bmatrix} \frac{1}{2} \rho U^2 B \left(K H_1^* \frac{\dot{h}}{U} + K H_2^* \frac{B \dot{a}}{U} + K^2 H_3^* \alpha + K^2 H_4^* \frac{h}{B} \right) \\ \frac{1}{2} \rho U^2 B^2 \left(K A_1^* \frac{\dot{h}}{U} + K A_2^* \frac{B \dot{a}}{U} + K^2 A_3^* \alpha + K^2 A_4^* \frac{h}{B} \right) \end{bmatrix} \quad (13)$$

where L and M are the lift and torque of deck, ρ is the air density, U is the average wind speed, B is the section width, $K = \omega B/U$ represents the dimensionless reduced frequency, ω represents the circular frequency of structural motion, $H_1^*-H_4^*$ and $A_1^*-A_4^*$ are non-dimensionless flutter derivatives for the deck. The flutter derivatives were identified in the TJ-7

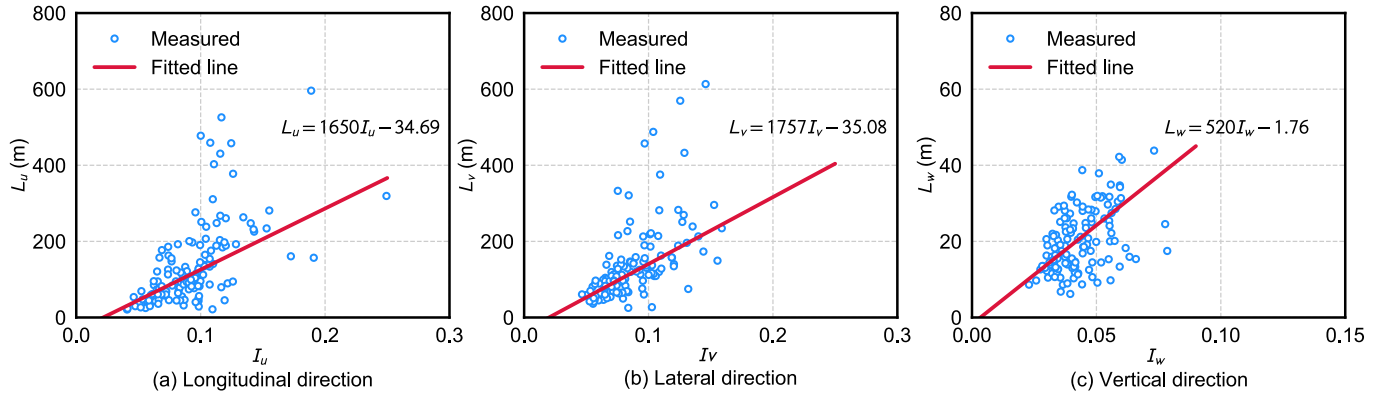


Fig. 9. Fitting curves of turbulence integral scale and turbulence intensity.

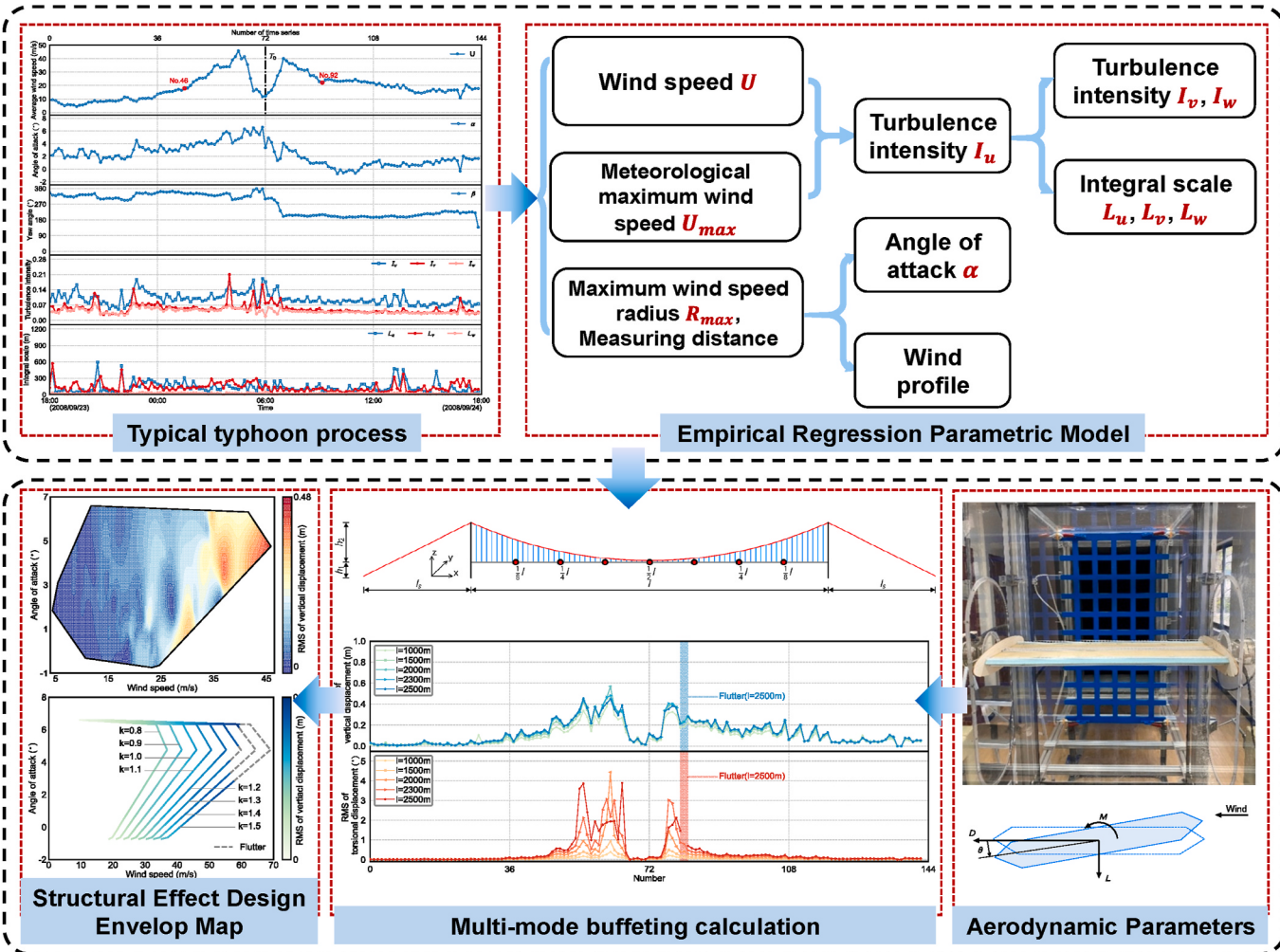


Fig. 10. Modeling of typhoon field and bridge buffeting response evolution.



Fig. 11. Layout of the TJ-7 wind tunnel.

wind tunnel. The wind AoA of typhoon “Hagupit” is from -1° to 6.6° , and all flutter derivatives were obtained at possible AoA range, and the results are shown in Fig. 18.

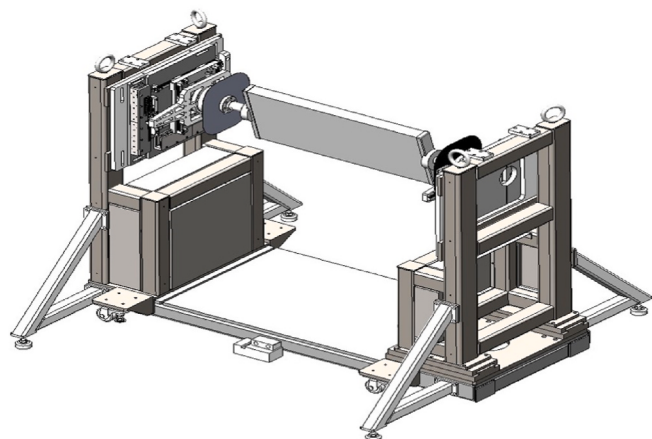
3.4. Aerodynamic admittances

The passive control grid was used for the experiment. Zhu et al. (2015) gave the effect of grid design parameters on the turbulence field characteristics through the test in the TJ-1 wind tunnel, and provided the design basis for the layout of the grid turbulence field. According to

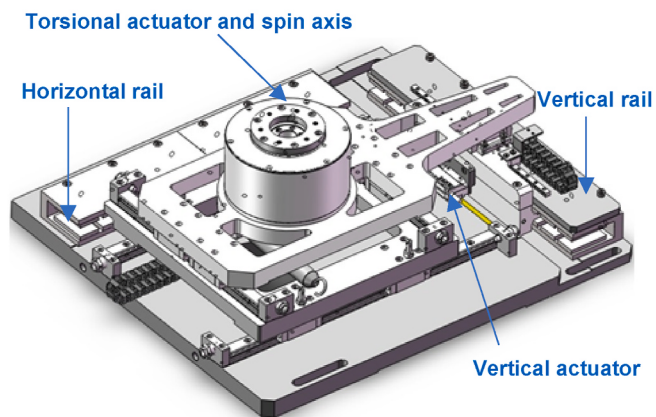
the relevant evidence in the above literature, three grids of different sizes were designed and fabricated to simulate the turbulent flow field.

The width of the grid spoiler bar is denoted as M , and the square spacing between two adjacent spoiler bars of the grid is denoted as N , as shown in Fig. 19. The grid blocking rate is recorded as P . The grid design schemes and parameters are shown in Table 5.

The buffeting force model and the buffeting force formula are:



(a) Schematic diagram of the forced vibration device



(b) Driving and decoupling systems of three DOFs

Fig. 12. Forced vibration device.

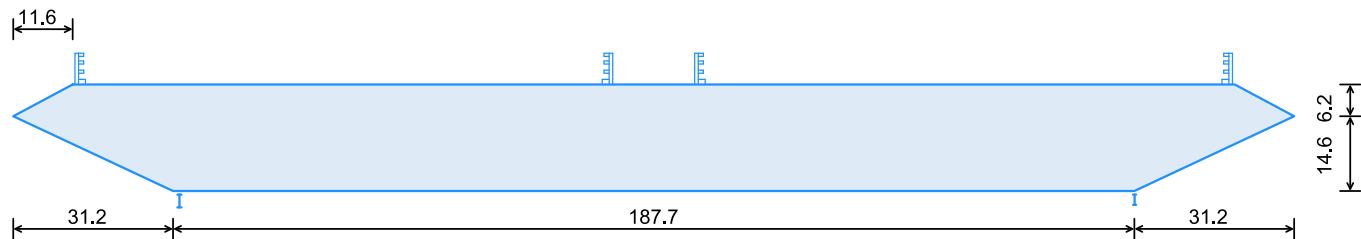


Fig. 13. Dimension definition of bridge section (mm).

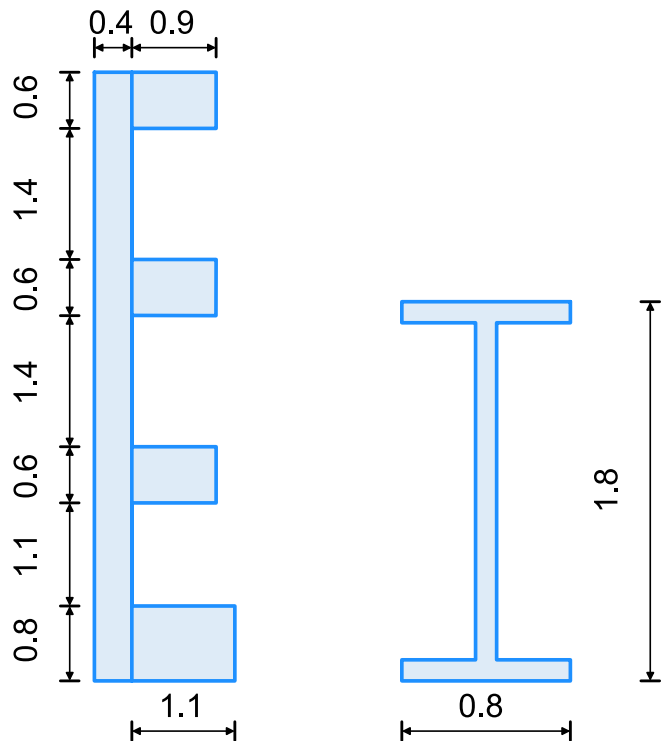


Fig. 14. Dimension definition of railing and track (mm).



Fig. 15. Model installation in the TJ-7 wind tunnel.

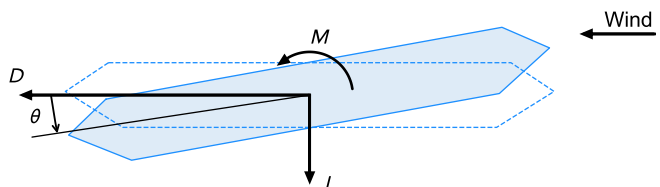
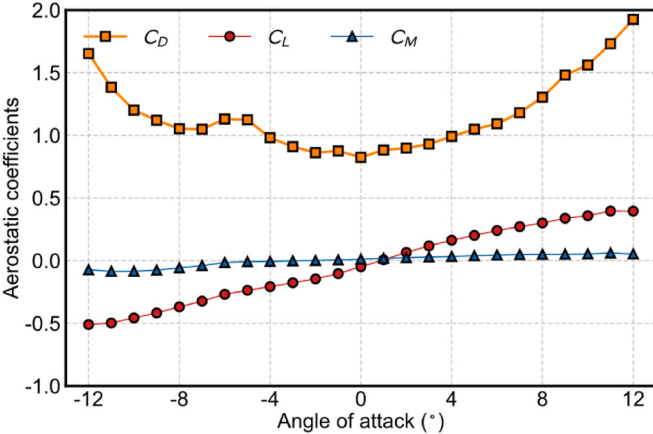
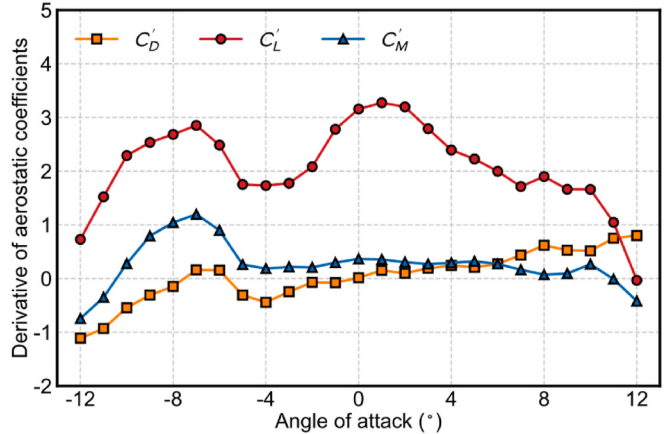


Fig. 16. Force direction definition.



(a) Aerodynamic coefficients



(b) Derivative of aerodynamic coefficients

Fig. 17. Aerostatic coefficients and their derivatives for different angles of attack.

$$\left\{ \begin{array}{l} D_b(t) = \frac{1}{2} \rho U^2 B \left[2C_{D\chi_{Du}} \frac{u(t)}{U} + (C_D + C_L)\chi_{Dw} \frac{w(t)}{U} \right] \\ L_b(t) = \frac{1}{2} \rho U^2 B \left[2C_{L\chi_{Lu}} \frac{u(t)}{U} + (C_L + C_D)\chi_{Lw} \frac{w(t)}{U} \right] \\ M_b(t) = \frac{1}{2} \rho U^2 B^2 \left[2C_{M\chi_{Mu}} \frac{u(t)}{U} + C_{M\chi_{Mw}} \frac{w(t)}{U} \right] \end{array} \right. \quad (14)$$

where χ is the aerodynamic admittance function related to lift, drag, and torque, u and w are the turbulence components in longitudinal and vertical directions, respectively, C_L , C_D , C_M , C'_L , C'_D and C'_M are the static aerodynamic coefficients and their derivatives (derivatives to the wind AoA), respectively. The self-power spectrum calculation is performed on both sides, and the cross spectrum is ignored, the buffeting force spectrum can be obtained, and the aerodynamic admittance function can be solved:

$$\left\{ \begin{array}{l} |\chi_{Du}(\omega)|^2 = |\chi_{Dw}(\omega)|^2 = \frac{4S_D(\omega)}{\rho^2 U^2 B^2 \{ 4C_D^2(\alpha)S_u(\omega) + [C_D(\alpha) - C_L(\alpha)]^2 S_w(\omega) \}} \\ |\chi_{Lu}(\omega)|^2 = |\chi_{Lw}(\omega)|^2 = \frac{4S_L(\omega)}{\rho^2 U^2 B^2 \{ 4C_L^2(\alpha)S_u(\omega) + [C_L(\alpha) + C_D(\alpha)]^2 S_w(\omega) \}} \\ |\chi_{Mu}(\omega)|^2 = |\chi_{Mw}(\omega)|^2 = \frac{4S_M(\omega)}{\rho^2 U^2 B^4 \{ 4C_M^2(\alpha)S_u(\omega) + C_M^2(\alpha)S_w(\omega) \}} \end{array} \right. \quad (15)$$

where S_D , S_L and S_M are the power spectrum functions of aerodynamic drag, lift and torque. The identification of aerodynamic admittance functions was also carried out in the TJ-7 wind tunnel. The test used grid to generate the turbulent flow field. The grid and bridge model are shown in Fig. 20.

The turbulence intensity of wind speed above 20 m/s is mainly considered. Fig. 21 shows a maximum turbulence of 14.7% and a minimum one intensity of 7.5% at high wind speeds observed during typhoon "Hagupit" process. The aerodynamic admittance is identified under these I_u range. The equivalent aerodynamic admittance identification method based on equivalent auto-spectrum method is used to compare it with Sears function with the oncoming wind flow 9 m/s. After calculating the measured equivalent aerodynamic admittance, a logarithmic third-order polynomial is used to fit the measured discrete points:

$$\log_{10}(S_K(n)) = \sum_0^3 (a_i \log_{10}(2\pi n B / U)), K = D, L, M \quad (16)$$

where n is the frequency, a_i is the parameter to be fitted, and S_K is the

drag, lift or torque spectrum. The fitting result is shown in Table 6 and the aerodynamic admittance identification result at 0° AoA is shown in Fig. 22.

The deviation between the equivalent aerodynamic admittance and Sears function is large in the low frequency band, and the error is reduced in the high frequency band. The overall trend is that the equivalent aerodynamic admittance decreases as the reduction frequency increases. The value of the lift equivalent aerodynamic admittance is lower than the result of Sears function, while the drag equivalent aerodynamic admittance and the torque equivalent aerodynamic admittance fluctuate around the value of Sears function, and the high frequency band is basically in the center of Sears curve. At the same time, it can be found that the fluctuation of the drag aerodynamic admittance is smaller than the other two aerodynamic admittance results, which is because the drag caused by the along-wind direction is larger than the lift caused by the vertical wind direction. Since the modal frequencies of long-span bridges used for buffeting calculation are all less than 0.5 Hz, the low-frequency data are mainly considered in the aerodynamic admittance fitting process.

4. Buffeting calculates of long-span bridges

4.1. Buffeting force model

The basic buffeting procedure is briefly introduced in this section, and more detailed formulations can be found in literature (Katsuchi et al., 1998), (Viseth et al., 2010). The analysis is based on the solution of the fully coupled system of equations of motion, where the bridge displacements are represented in generalized coordinates of the mode shapes in still-air. The multimode system of equations of motion including the aeroelastic effects is written in frequency domain as:

$$\tilde{M}_0 G_{\eta}(\omega) + [\tilde{C}_0 - \tilde{C}_{ae}(U, \omega)] G_{\dot{\eta}}(\omega) + [\tilde{K}_0 - \tilde{K}_{ae}(U, \omega)] G_{\ddot{\eta}}(\omega) = G_{Q_{buff}}(\omega) \quad (17)$$

where ω = circular frequency; \tilde{M}_0 , \tilde{K}_0 , and \tilde{C}_0 = generalized mass, stiffness, and damping matrices in still-air, respectively; \tilde{C}_{ae} and \tilde{K}_{ae} = generalized aeroelastic damping and stiffness matrices, respectively; G_{η} , $G_{\dot{\eta}}$, and $G_{\ddot{\eta}}$ = Fourier transforms of the acceleration, velocity, and displacement responses in generalized coordinates, respectively; and $G_{Q_{buff}}$ = generalized buffeting force. According to random vibration theory, the PSD matrices of the generalized displacement response $[\tilde{S}_R(\omega)]$ and the buffeting force $[S_{Q_{buff}}(\omega)]$ are related as follows:

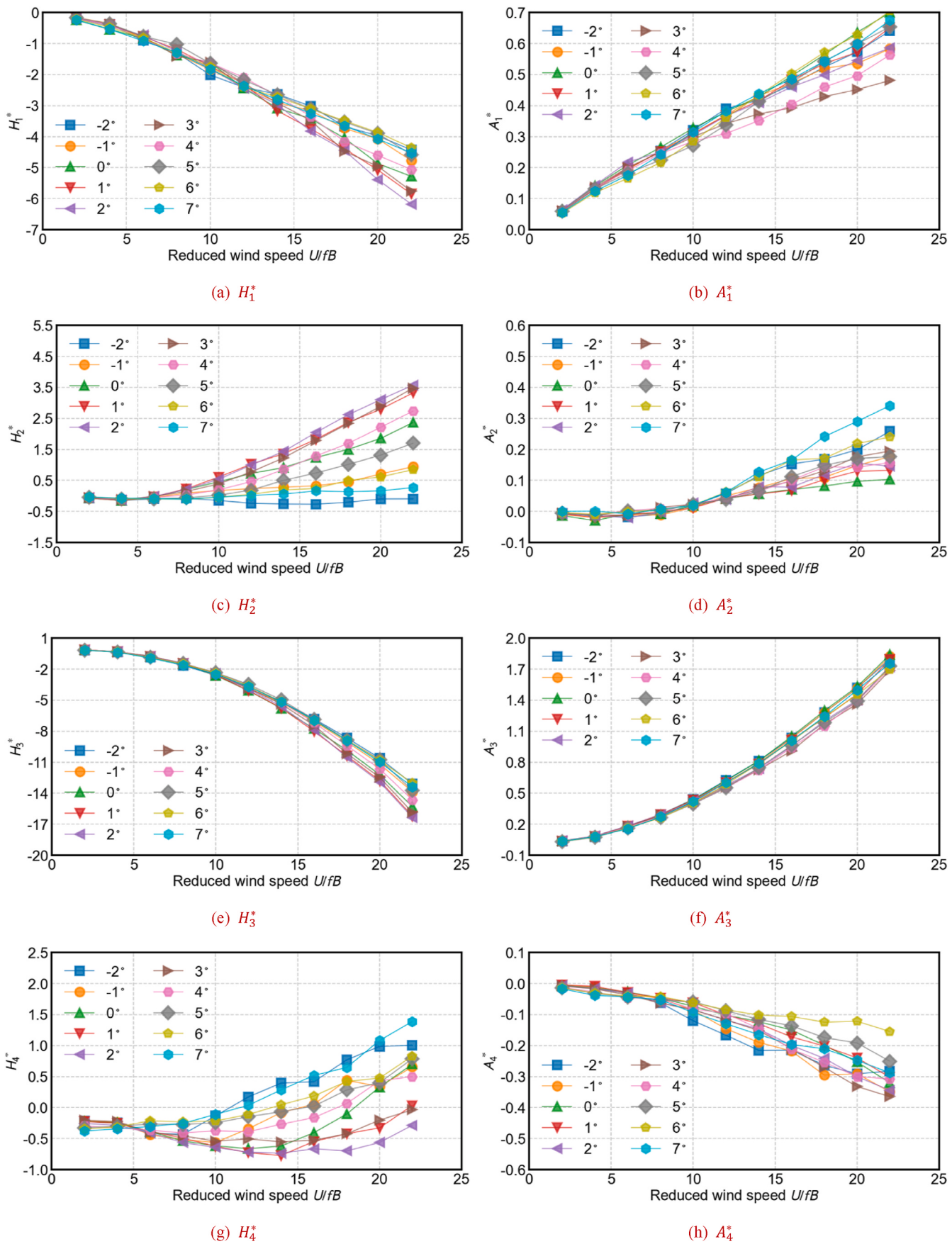


Fig. 18. Flutter derivatives at different AoAs.

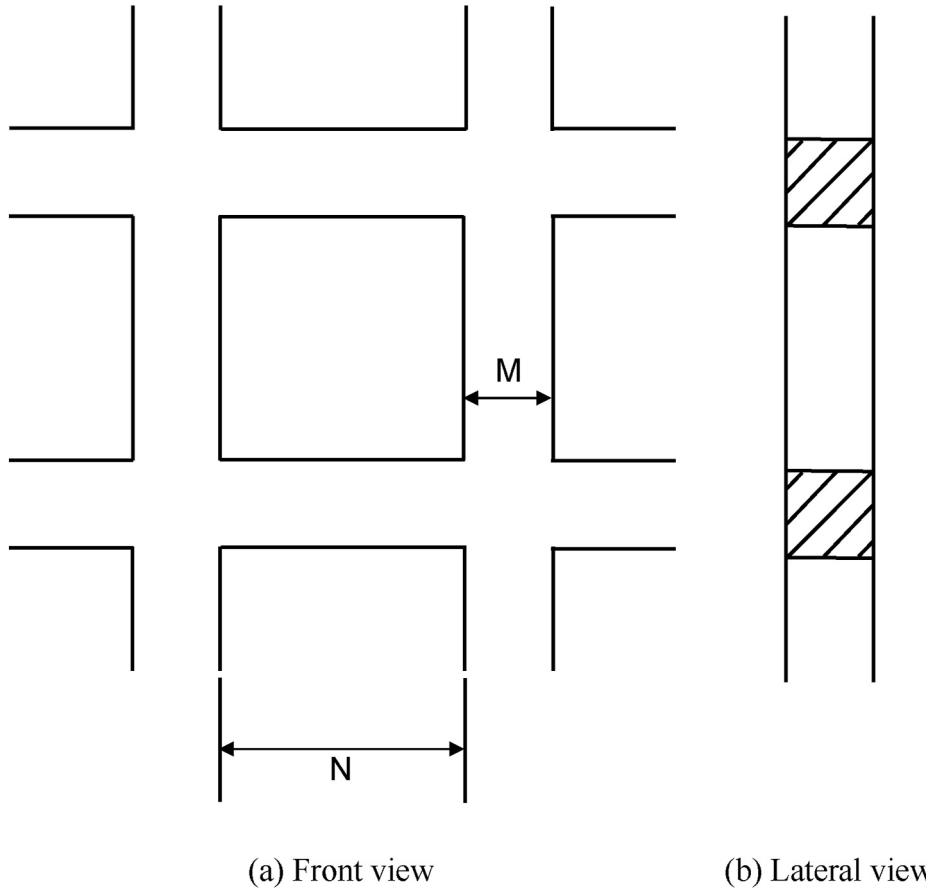


Fig. 19. Schematic of typical structure of square grids.

Table 5
Design schemes and parameters of grids.

Case	M(mm)	N(mm)	P(%)
grid 1	135	20	26.6
grid 2	85	20	38.5
grid 3	85	30	45.6

$$[\tilde{S}_R(\omega)] = [E_\eta^{-1}(\omega) S_{Q_{buff}}(\omega) E_\eta^{-1*}(\omega)] \quad (18)$$

$$E_\eta(U, \omega) = \{-\tilde{M}_0\omega^2 + [\tilde{C}_0 - \tilde{C}_{ae}(U, \omega)]\}i\omega + [\tilde{K}_0 - \tilde{K}_{ae}(U, \omega)] \quad (19)$$

The frequency-dependent generalized aeroelastic stiffness and damping matrices can be obtained by:

$$\tilde{K}_{ae}(U, \omega) = \int [\Phi^T K_{ae}(U, \omega) \Phi] dx \quad (20)$$

$$\tilde{C}_{ae}(U, \omega) = \int [\Phi^T C_{ae}(U, \omega) \Phi] dx \quad (21)$$

In the previous expressions, $\varphi_i = [\phi_y, \phi_z, \phi_\theta]^T$ is the mode shape vector; Φ denotes the matrix of the mode shapes. Having established the system matrices, the buffeting action needs to be defined. The elements of the spectral matrix of the buffeting force can be written in generalized coordinates as:

$$S_{Q_{buff}}(\omega) = \iint \Phi^T(x_1) B_1(\omega) S_V(\Delta x, \omega) B_q^T(\omega) \Phi(x_2) dx_1 dx_2 \quad (22)$$

$$S_V(\Delta x, \omega) = \begin{bmatrix} S_{uu}(\Delta x, \omega) & S_{uw}(\Delta x, \omega) \\ S_{uw}(\Delta x, \omega) & S_{ww}(\Delta x, \omega) \end{bmatrix} \quad (23)$$

$$S_V(\Delta x, \omega) = \begin{bmatrix} S_u(\omega) & 0 \\ 0 & S_w(\omega) \end{bmatrix} \times \begin{bmatrix} C_u(\Delta x, \omega) & 0 \\ 0 & C_w(\Delta x, \omega) \end{bmatrix} \quad (24)$$

where $S_V(\Delta x, \omega)$ = cross-spectral density matrix containing the auto-spectral and cross-spectral densities of the turbulence components at the two points x_1 and x_2 , which are separated by a distance of Δx . $C_a(\Delta x, \omega)$ ($a = u, v, w$) is the normalized cross-spectral densities for Δx . And the normalized cross-spectral density in the conventional form as:

$$C_a(\Delta x, \omega) = \exp\left(-\frac{c\Delta x}{l}\right) \quad (25)$$

where the $c = 7Kl/2\pi B$, $K = \omega B/U$ (Jain et al., 1996). And the matrix $B_q(\omega)$ includes the steady-state force coefficients:

$$B_q(\omega) = \frac{\rho UB}{2} \begin{bmatrix} 2(D/B)\bar{C}_D \chi_{Du} & [(D/B)C'_D - C_L] \chi_{Dw} \\ 2\bar{C}_L \chi_{Lu} & [C_L + (D/B)\bar{C}_D] \chi_{Lw} \\ 2B\bar{C}_M \chi_{Mu} & BC'_M \chi_{Mw} \end{bmatrix} \quad (26)$$

where \bar{C}_D , \bar{C}_L , and \bar{C}_M = mean values of the steady-state force coefficients associated with the drag, lift, and torque, respectively; C'_D , C'_L , and C'_M are the corresponding derivatives; and D = girder height. And the aerodynamic admittance is obtained from wind tunnel test. Finally, the RMS acceleration response can be obtained from the displacement spectra using:

$$\sigma_R = \sqrt{\int_0^\infty S_{\ddot{R}}(\omega) d\omega}, S_{\ddot{R}}(\omega) = \omega^4 [\Phi(\omega) \tilde{S}_R(\omega) \Phi^T(x)] \quad (27)$$

where $S_{\ddot{R}}(\omega)$ and $S_R(\omega)$ are the acceleration and displacement spectra in

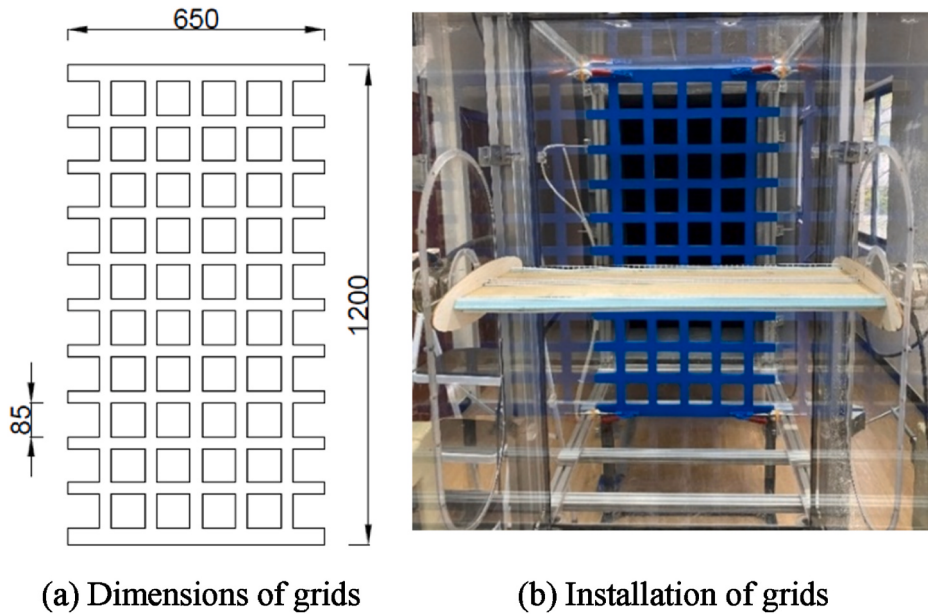
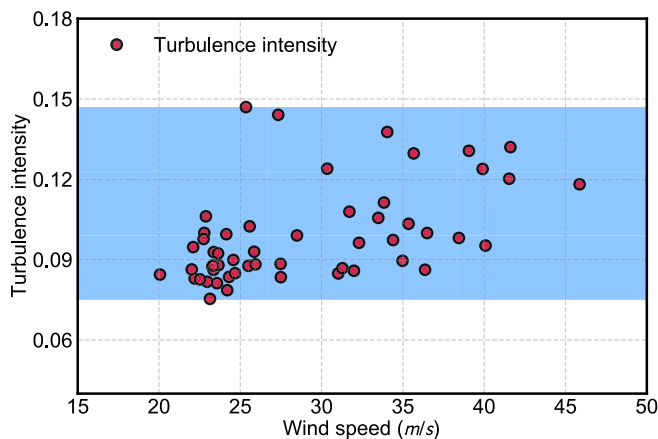


Fig. 20. Dimensions and installation of grids (Unit: mm).

Fig. 21. Turbulence intensity range at high wind speed ($\geq 20 \text{ m/s}$).

global coordinates, respectively. It should be noted that there will be an almost infinite resonance response when the singular value of the transfer function matrix $E_\eta(U, \omega)$ has a minimum value, which indicates that the bridge structure diverges and no longer has stability.

4.2. Dynamic characters of suspension bridge with different spans

Five different finite element models of suspension bridges with main spans of 1000, 1500, 2000, 2300 and 2500 m were established, and the multi-mode coupling buffeting frequency domain analysis was carried out for streamlined box girders according to the wind characteristics of typhoon "Hagupit". Because of the different bridge spans, the bridge tower heights also varied. Apart from the bridge spans and tower heights, other structural parameters and aerodynamic factors related to the bridge section remained consistent for the five different models. The bridge and coordinates are shown in Fig. 23. The consistent parameters for the different bridge models are shown in Table 7.

l is the length of main span from 1500 m to 2500 m, l_s is the length of side span which is kept at 0.3 l . h_1 is the height from the deck to the foundation, h_2 is the height from the top of the tower to deck, and they are reasonably determined according to the rise-span ratio of 1/11. The finite-element analysis was conducted using the ANSYS platform. Three-

Table 6
Fitting parameters of aerodynamic admittance under different AoA.

Aerodynamic admittance	AoA ($^\circ$)	a_0	a_1	a_2	a_3
Drag	-1	-0.552	-0.421	-0.401	-0.404
	0	-0.616	-0.402	-0.445	-0.342
	1	-0.570	-0.470	-0.545	-0.422
	2	-0.593	-0.543	-0.576	-0.389
	3	-0.620	-0.635	-0.648	-0.288
	4	-0.529	-0.630	-0.580	-0.223
	5	-0.377	-0.686	-0.618	-0.137
	6	-0.364	-0.507	-0.751	-0.354
	7	-0.381	-0.372	-0.826	-0.402
	-1	-0.796	-1.263	-0.438	0.274
	0	-0.755	-1.215	-0.411	0.277
	1	-0.721	-1.267	-0.339	0.355
	2	-0.760	-1.281	-0.392	0.396
	3	-0.800	-1.213	-0.339	0.439
Lift	4	-0.720	-1.222	-0.239	0.493
	5	-0.584	-1.089	-0.382	0.344
	6	-0.546	-0.751	-0.640	-0.095
	7	-0.547	-0.588	-0.736	-0.141
	-1	-0.498	-0.526	-0.609	-0.349
	0	-0.461	-0.439	-0.655	-0.396
	1	-0.438	-0.362	-0.667	-0.474
	2	-0.457	-0.244	-0.737	-0.555
	3	-0.403	-0.130	-0.744	-0.634
	4	-0.330	-0.180	-0.668	-0.535
	5	-0.329	-0.127	-0.555	-0.599
	6	-0.418	-0.253	-0.494	-0.447
	7	-0.484	-0.272	-0.442	-0.455

dimensional Euler beam elements with axial stiffness were used to model the bridge towers with rigid lateral arms. Tensile link elements were employed to model the suspended cables and hangers. The main bridge girder was also modeled using Euler beam elements and connected to hangers through a rigid "fishbone" framework. The bridge girders and suspension cables were discretized at the hanger locations. Because the bridge towers had a uniform section, the towers were discretized at the elevations of bridge girders and horizontal connectors. The bases of bridge towers were considered as fixed ends, and the two free ends of bridge girders as vertically supported.

Additionally, the bridge girders and towers were connected through the longitudinal axis with vertical restrictions. Large displacement effects were considered, and the Newton-Raphson algorithm was

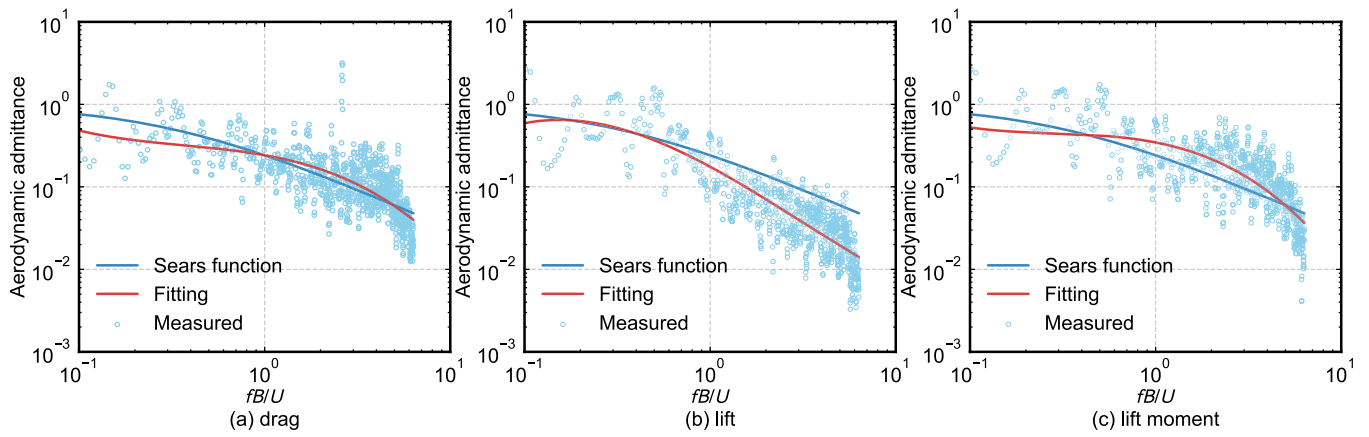
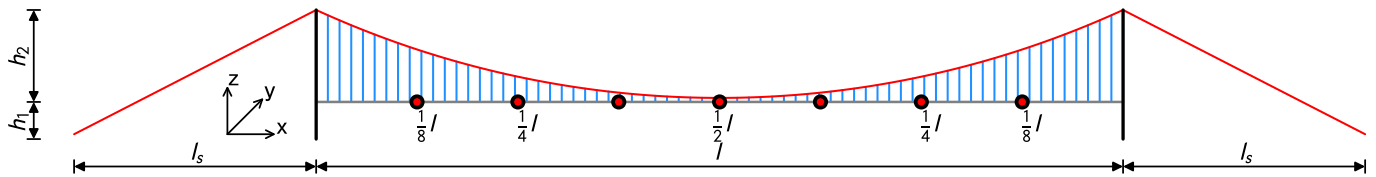
Fig. 22. Aerodynamic admittance identification result (0° AoA).

Fig. 23. Elevation view of bridge layout for adjustable main spans.

Table 7
Structural parameters of adjustable span bridge models.

Parameters	Values
Main span l (m)	1000, 1500, 2000, 2300, 2500
Sag/span ratio h_2/l	1/11
Deck width B (m)	44.8
Deck thickness D (m)	3
Suspender gap (m)	20
Mass per unit length m (kg/m)	22000
Mass moment of inertia long longitudinal axis per unit length I (kg \cdot m ² /m)	2210000
Structural damping ratio ξ	0.005

employed to calculate the geometric nonlinearity. Equivalent initial strain was applied to suspension cables and hangers as the pre-tension in link elements.

The fundamental frequencies of five bridge models with different spans are given in Table 8 with different bridge spans and tower sizes. It should be noted that, owing to the long bridge span, both of the first vertical and torsional mode shapes are antisymmetric for all analyzed bridge models with five span lengths. The dependences of the first

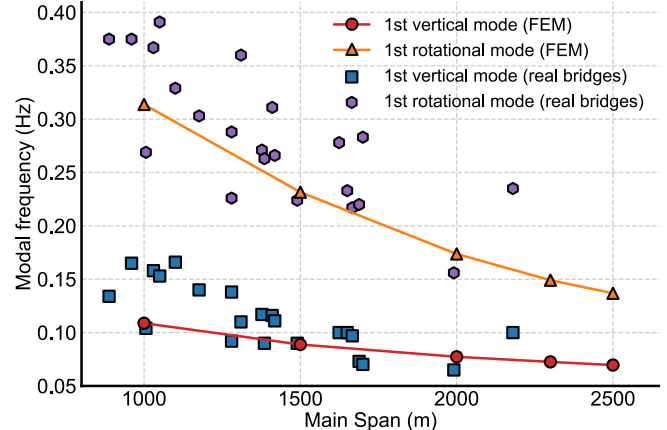


Fig. 24. Vertical and torsional dynamic characteristics for different main span lengths of bridges.

vertical and torsional frequencies on the main span length of long-span bridges are plotted in Fig. 24. The dynamic characteristics of many real bridges were studied by Ding et al. (2023).

Table 8
Bridge span, tower height, and parameters of six bridge models.

l (m)	l_s (m)	h_1 (m)	h_2 (m)	1st AV(Hz)	1st SV(Hz)	2nd SV(Hz)	2nd AV(Hz)	1st AT(Hz)	1st ST(Hz)	Diameter of Cable (m)
1000	300	28.2	94	0.1088	0.1609	0.2160	0.2580	0.3138	0.3537	0.65
1500	450	41.85	139.5	0.0888	0.1201	0.1611	0.1971	0.2316	0.2408	0.70
2000	600	46.25	185	0.0773	0.1033	0.1381	0.1671	0.1737	0.1888	0.85
2300	690	53.015	212.06	0.0725	0.0965	0.1289	0.1550	0.1491	0.1672	0.95
2500	750	57.625	230.5	0.0696	0.0923	0.1233	0.1483	0.1369	0.1542	1.01

AV is asymmetric vertical mode.

SV is symmetric vertical mode.

AT is asymmetric torsional mode.

ST is symmetric torsional mode.

4.3. Structural response calculation

According to the wind parameter model summarized at typhoon “Hagupi”, other wind parameters are related to the wind speed after the measured wind speed is determined as shown in Eqs. (10) and (11) and ERPM model. Fig. 25 shows the AoA, turbulence intensity I_u , I_w , integral scale L_u and L_w calculated by the wind parameter model. The results show that the AoA calculated by the model is in good agreement with the measured AoA, while other wind parameters are in good agreement with most of the measured data, but it is difficult to simulate the points with high turbulence intensity and integral scale.

The wind field parameters calculated by the ERPM model were used in the buffeting response analysis of long-span bridges. For the fluctuating wind spectrum, the fitted von Kármán spectrum under the measured integral scale was used, and the recognized aerodynamic

admittance was considered during the calculation process. The aerodynamic admittance at the wind speed above 20 m/s was based on the experimental results, and the aerodynamic admittance at the wind speed below 20 m/s was adopted using Sears function. The vertical and torsional responses are of more concern for long-span bridges, so the calculation process is mainly focused on the vertical and torsional models, and the lateral mode is ignored. In this study, the first four-order vertical modes and the first two torsional modes were calculated, and the mid-span, one-quarter span and one-eighth span were selected for analysis and calculation. The resulting response spectrum at maximum wind speed is shown in Fig. 26.

Under the maximum wind speed during the typhoon, the vertical buffeting response of the bridge presents the characteristics of multi-modal contribution. The maximum vertical response is located at the 1/4 span position, and the maximum amplitude of the response

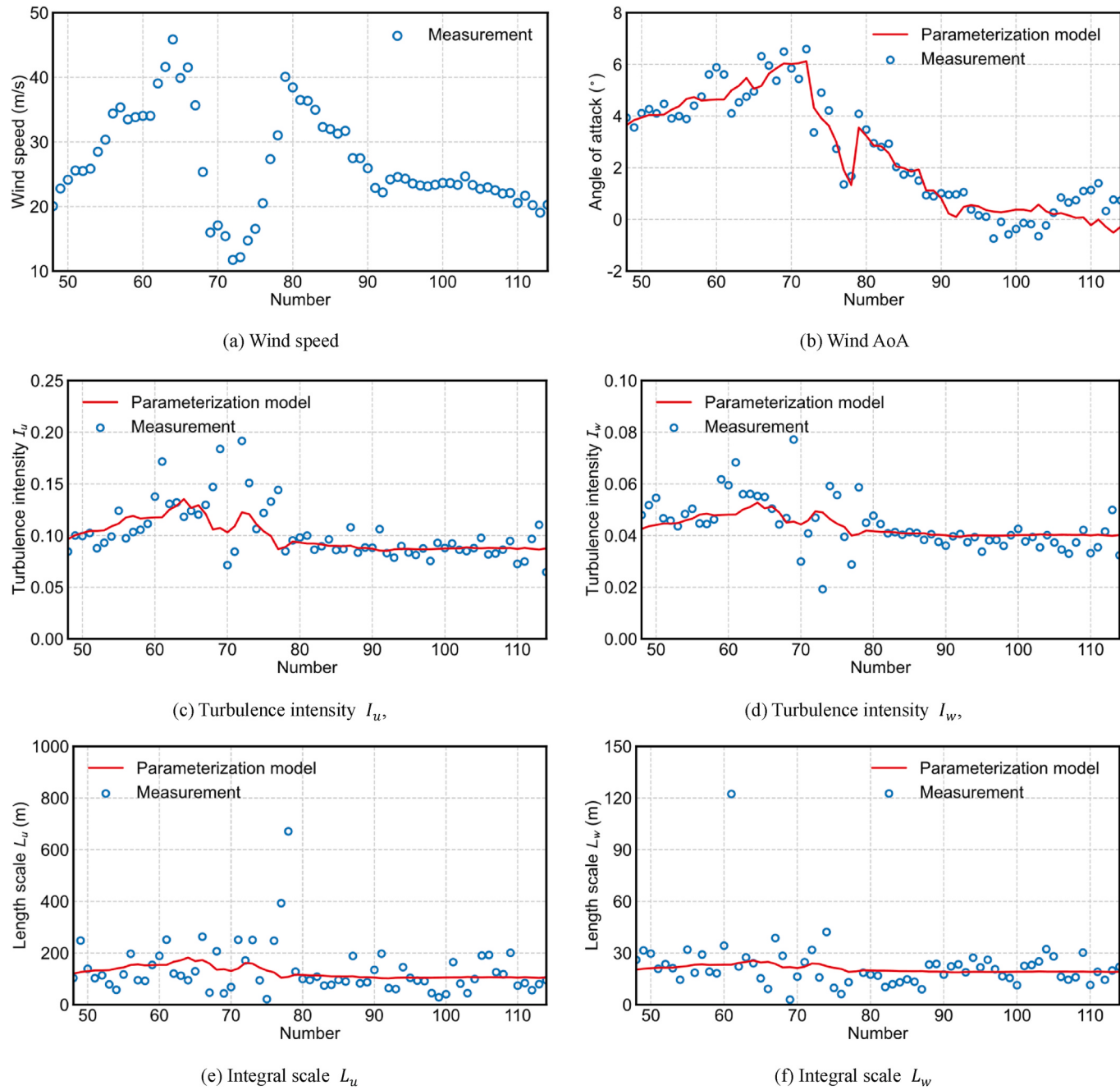


Fig. 25. Comparison between fitting typhoon field parameters and measured data.

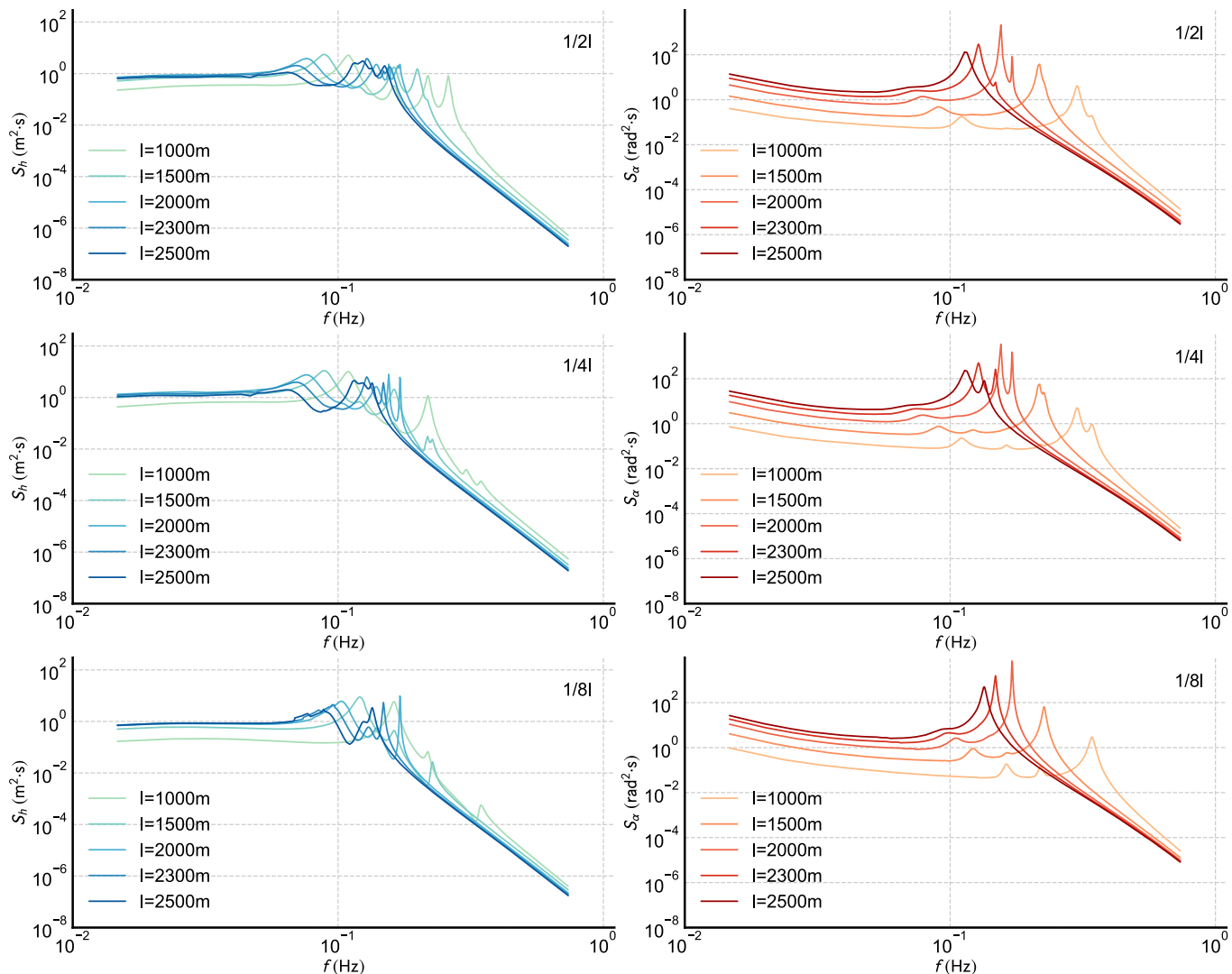


Fig. 26. Buffeting response spectrum with different spans at different span locations (maximum wind speed 45.86 m/s).

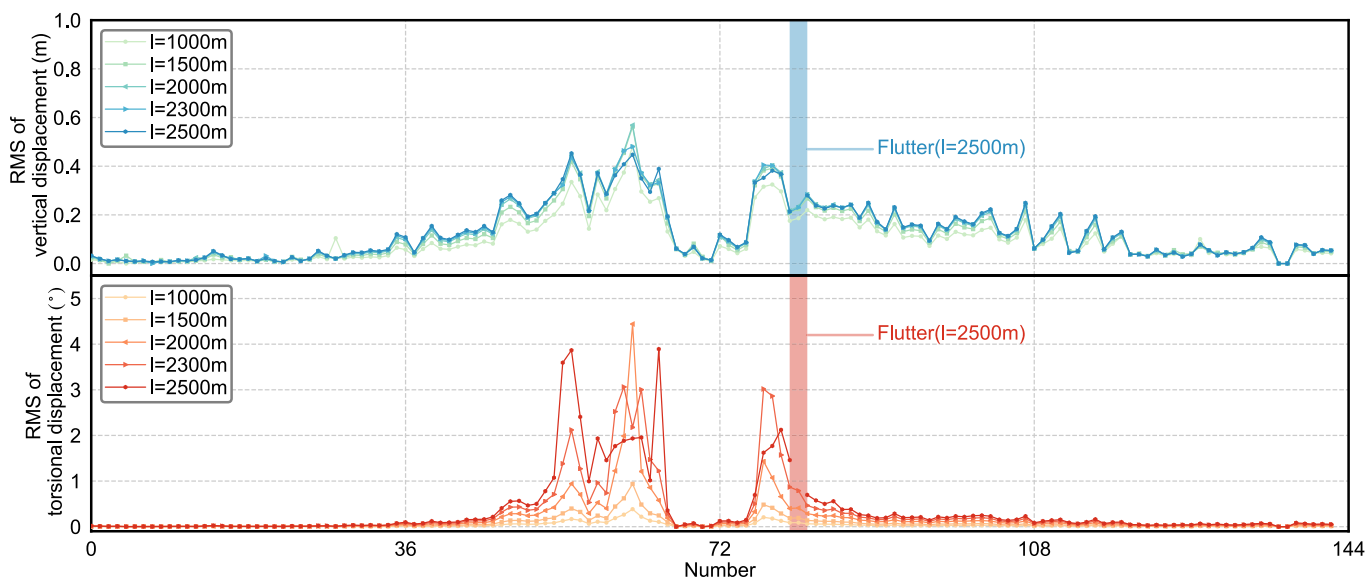


Fig. 27. Comparison of bridge buffeting responses with different spans and suggested values for code.

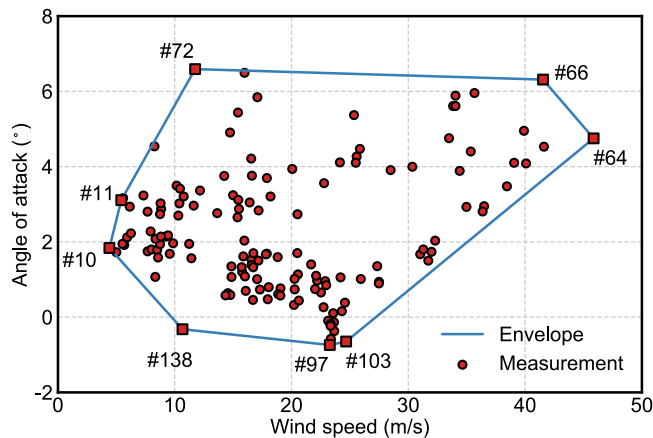


Fig. 28. Measured data envelope of “Hagupit” characteristics.

spectrum appears in the 2500 m span bridge, but it is not much different from the response of other span bridges. Contrary to the vertical response, the maximum amplitude of the torsional buffeting response is not the bridge with the largest span. The background component in the torsional buffeting response gradually increases as the bridge span increases. However, with the reduction of the natural frequency of the bridge, the resonance component gradually decreases after 2000 m, and the torsional response decreases with the same tendency.

The buffeting response of the 1/4 span under the whole typhoon process is shown in Fig. 27. It is clear found that the vertical buffeting response of the bridge changes with the wind speed, showing an “M” type trend, and the maximum response occurs at the maximum wind speed. And it can be considered that the vertical buffeting response of the bridge has no obvious relationship with the span according to the results.

For bridges with spans less than 2000 m, the torsional response varies with wind speed and presents an M shaped trend, which is the same as the vertical response, and the maximum response is basically located at the maximum wind speed. But when the span is greater than 2000 m, the torsional response no longer becomes larger as the span increases, and the response is no longer completely related to the wind speed.

The envelope diagram of the relationship between wind speed and AoA under the typhoon process is drawn as shown in Fig. 28. And the

buffeting response results of the mid-span position of bridge with the span of 1500 m under “Hagupit” wind parameters are shown in Fig. 29. The results show that the buffet response is affected by both AoA and wind speed, and the response becomes larger as the wind speed increases. However, it should be noted that the maximum buffet response does not increase with the increase of AoA, there is the most unfavorable AoA. When the AoA is between 4° and 5°, the maximum response will occur at each wind speed, but the response will decrease if the AoA is larger or smaller. This phenomenon shows the joint influence from typhoon field parameters, and it should be noticed that the maximal response not always depends on the maximal oncoming wind velocity. The analysis procedure like about could be defined as structural effect design envelop map (EDEM) method.

On the other hand, the maximum wind speed corresponding to each AoA is the possible instability point under the AoA. And connecting these points is the maximum response boundary of the long-span bridge during a typhoon. The line between points #72, #66, #64, #103 and #97 in Fig. 28 is the potential instability boundary of the bridge for typhoon “Hagupit”. The possible typhoon processes with higher intensity levels can be calculated according to the proposed ERPM taking “Hagupit” as a standard typhoon, and the maximum buffeting response variation trend of bridges under different typhoons can be obtained. Wind speed is the most direct criterion for distinguishing typhoon processes. In order to obtain the wind characteristic parameters of larger typhoon processes that may exist, the “Hagupit” ratio is used as a standard typhoon, and the turbulence intensity and integral scale at the wind speed of 1.0–1.5 times the “Hagupit” ratio was calculated according to the parametric model. Fig. 30 shows the possible instability boundary of a 1500 m span bridge under 1.0–1.5 times the standard typhoon process, and k represents the magnification of the “Hagupit” typhoon wind speed.

The vertical and torsional buffeting responses of the bridge will become larger when the typhoon intensity becomes higher. The instability begins to appear near the maximum wind speed when $k = 1.3$, which shows that the bridge may be structurally damaged during the typhoon. And the range of instability boundary gradually increases when k continues to increase that means stronger typhoons are more likely to cause damage to bridge structures. And it can be found that the wind speed of bridge instability is always at nearly 60 m/s when the value of k changes, and slightly different at different AoAs. This is because the flutter critical wind speed of the bridge is stable and will not change with typhoon changes.

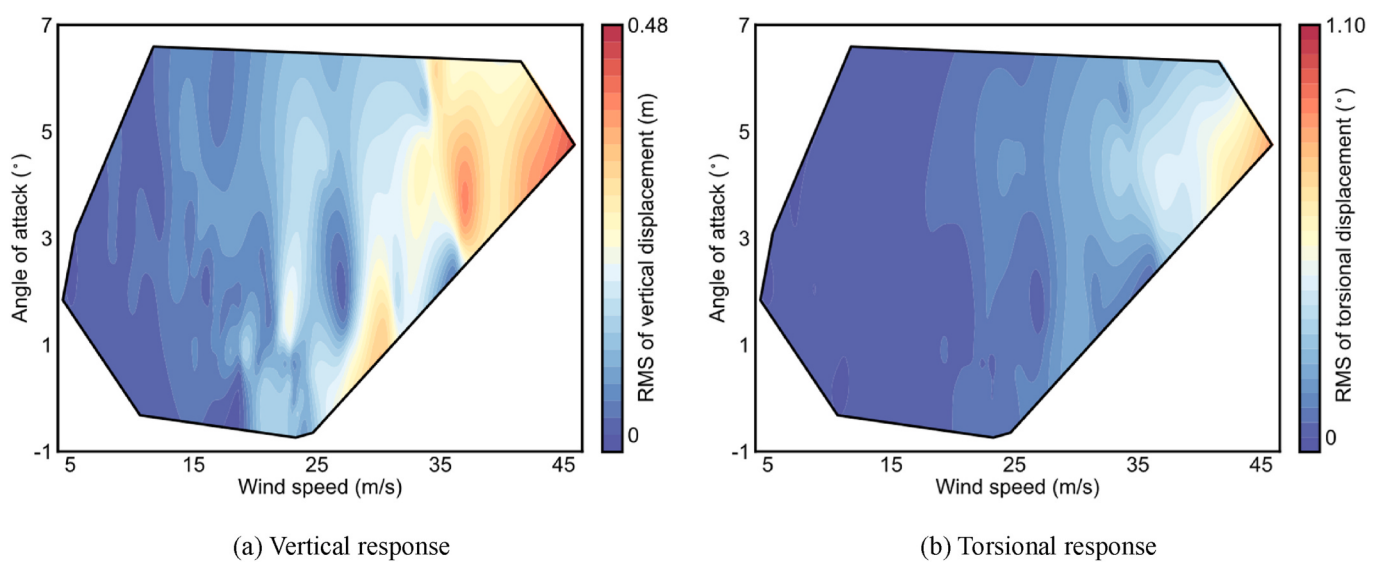


Fig. 29. Buffeting response of bridge with the span of 1500 m under “Hagupit” characteristics.

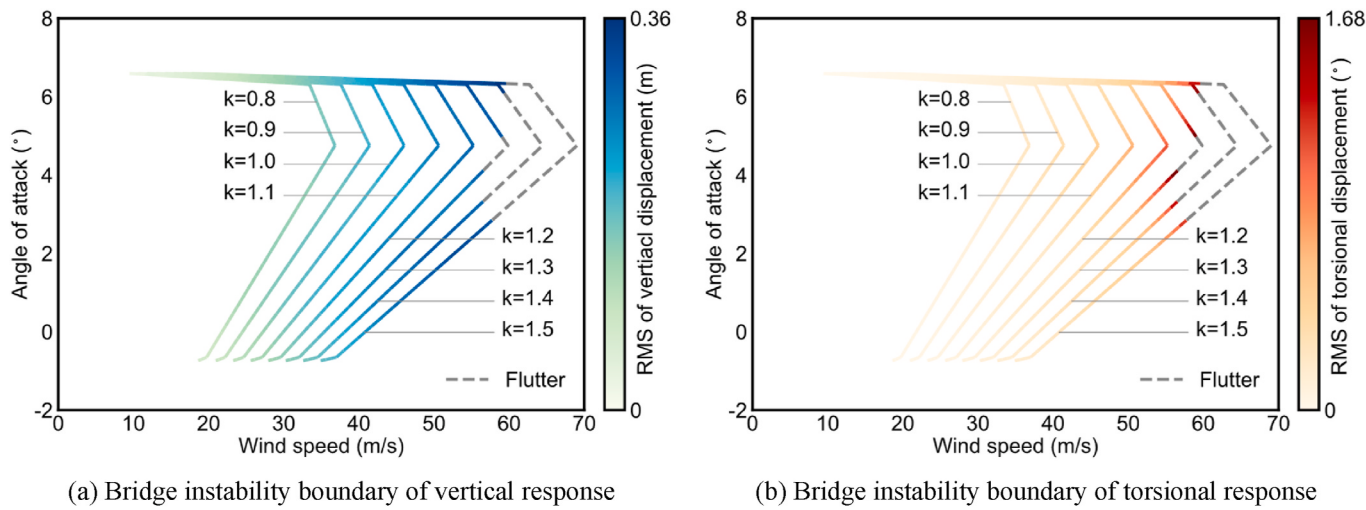


Fig. 30. Bridge instability boundary under different typhoon.

5. Conclusions

This study uses the measured typhoon "Hagupit" data to summarize the average wind speed, wind AoA, turbulence intensity, turbulence integral scale and fluctuating wind spectrum wind characteristic parameters, and a relationship model among related parameters called as ERPM was proposed. The aerodynamic parameters of long-span bridges were obtained through wind tunnel tests and the buffeting responses of bridges with different spans were calculated based on structural effect design envelope map (EDEM). The main conclusions are summarized as follows.

- (1) For central penetrating typhoons, there is an obvious positive probabilistic correlation between the wind AoA and the wind speed. The turbulence intensity before landfall showed a trend of first decreasing and then increasing with the increase of wind speed, and the turbulence intensity after landfall increased with the increase of wind speed. And there is a linear increase relationship between longitudinal and vertical turbulence intensity and the along-wind turbulence intensity. The turbulence integral scale is more discrete, but it has an approximate linear relationship with the turbulence intensity.
- (2) The vertical buffeting response presents the characteristics of multi-modal participation when the span of the bridge increases, while the torsional buffeting response gradually decreases when the span exceeds 2000 m. The difference in the vertical buffeting response of bridges with different spans is small during the entire typhoon landing process, and the maximum response occurs at the maximum wind speed.
- (3) The buffeting response usually increases with the increase of wind speed, but does not change monotonically with the change of AoA, and there is the most unfavorable AoA. The maximum wind speed is not the controlling condition of buffeting response, which reflects the complexity of the joint effects of multiple wind parameters during the typhoon process. Taking "Hagipit" as the standard typhoon, the proposed ERPM can be used to calculate typhoon processes of different intensity levels, and the changing trend of the maximum buffeting response of the bridge can be obtained. As the typhoon level increases, the buffeting response continues to increase, and the instability boundary range gradually increases. Under the action of typhoons of different intensity levels, the instability wind speed of the bridge is relatively stable.

The research taken "Hagupit" as an example, and the wind parameter model was established by summarizing the evolution of wind

characteristic parameters throughout the entire process of typhoon landing. The buffeting response calculation model under different wind parameters was established to provide a basis for the selection of wind loads by taking into account the multi-modal coupling effect. The typhoon used in this study is a typical typhoon process with central penetration characteristics, which has important reference value for the evaluation of extreme conditions of such typical strong typhoons. However, different typhoons and different landing locations may have the impact on the wind parameters of the typhoon. In future studies, if more typhoon parameters can be considered, the more universal model can be established.

CRediT authorship contribution statement

Lin Zhao: Resources. **Zilong Wang:** Validation. **Weile Chen:** Validation. **Wei Cui:** Methodology, Conceptualization.

Declaration of competing interest

The authors declare that they have no known competing financial interests or personal relationships that could have appeared to influence the work reported in this paper.

Data availability

Data will be made available on request.

Acknowledgements

The authors gratefully acknowledge the support of the National Key Research and Development Program of China (2021YFF0502200) and the National Natural Science Foundation of China (52478552, 52378527).

References

- Bucher, C.G., Lin, Y.K., 1990. Effects of wind turbulence on motion stability of long-span bridges. *J. Wind Eng. Ind. Aerod.* 36, 1355–1364.
- Bucher, C.G., Lin, Y.K., 1988. Stochastic stability of bridges considering coupled modes. *J. Eng. Mech.* 114 (12), 2055–2071.
- Cao, S.Y., Tamura, Y., Kikuchi, N., Saito, M., Nakayama, I., Matsuzaki, Y., 2009. Wind characteristics of a strong typhoon. *J. Wind Eng. Ind. Aerod.* 97 (1), 11–21.
- Cui, W., Zhao, L., Ge, Y.J., 2021. Non-Gaussian turbulence induced buffeting responses of long-span bridges. *J. Bridge Eng.* 26 (8), 04021057.
- Cui, W., Zhao, L., Ge, Y.J., 2022. Non-Gaussian turbulence induced buffeting responses of long-span bridges based on state augmentation method. *Eng. Struct.* 254, 113774.
- Davenport, A.G., 1962. Buffeting of a suspension bridge by storm winds. *J. Struct. Div.* 88 (3), 233–270.

- Ding, Y.J., Zhao, L., Xian, R., Liu, G., Xiao, H.Z., Ge, Y.J., 2023. Aerodynamic stability evolution tendency of suspension bridges with spans from 1000 to 5000 m. *Front. Struct. Civ. Eng.* 17 (10), 1465–1476.
- Fang, G.S., Pang, W.C., Zhao, L., Rawal, P., Cao, S.Y., Ge, Y.J., 2021. Toward a refined estimation of typhoon wind hazards: parametric modeling and upstream terrain effects. *J. Wind Eng. Ind. Aerod.* 209, 104460.
- Fenerci, A., Øiseth, O., 2018. Strong wind characteristics and dynamic response of a long-span suspension bridge during a storm. *J. Wind Eng. Ind. Aerod.* 172, 116–138.
- Ge, Y.J., Zhao, L., 2014. Wind-excited stochastic vibration of long-span bridge considering wind field parameters during typhoon landfall. *Wind Struct.* 19 (4), 421–441.
- Hu, L., Xu, Y.L., Huang, W.F., 2013. Typhoon-induced non-stationary buffeting response of long-span bridges in complex terrain. *Eng. Struct.* 57, 406–415.
- Huang, Z., Xu, Y.L., Zhan, S., 2021. Conditionally simulating nonstationary typhoon winds with time-varying coherences for long-span bridges. *J. Wind Eng. Ind. Aerod.* 212, 104599.
- Hui, Y., Li, B., Kawai, H., Yang, Q.S., 2017. Non-stationary and non-Gaussian characteristics of wind speeds. *Wind Struct.* 24 (1), 59–78.
- Ishizaki, H., 1983. Wind profiles, turbulence intensities and gust factors for design in typhoon-prone regions. *J. Wind Eng. Ind. Aerod.* 13 (1–3), 55–66.
- Isyumov, N., Alan, G., 2012. Davenport's mark on wind engineering. *J. Wind Eng. Ind. Aerod.* 104, 12–24.
- Jain, A., Jones, N.P., Scanlan, R.H., 1996. Coupled flutter and buffeting analysis of long-span bridges. *J. Struct. Eng.* 122 (7), 716–725.
- Jones, N.P., Scanlan, R.H., 2001. Theory and full-bridge modeling of wind response of cable-supported bridges. *J. Bridge Eng.* 6 (6), 365–375.
- Katsuchi, H., Jones, N.P., Scanlan, R.H., Akiyama, H., 1998. Multi-mode flutter and buffeting analysis of the Akashi-Kaikyo bridge. *J. Wind Eng. Ind. Aerod.* 77, 431–441.
- Katsuchi, H., Jones, N.P., Scanlan, R.H., 1999. Multimode coupled flutter and buffeting analysis of the Akashi-Kaikyo Bridge. *J. Struct. Eng.* 125 (1), 60–70.
- Lei, S.M., Ge, Y.J., Li, Q., Thompson, D.J., 2023. Frequency-domain method for non-stationary stochastic vibrations of train-bridge coupled system with time-varying characteristics. *Mech. Syst. Signal Process.* 183, 109637.
- Li, L.X., Kareem, A., Xiao, Y.Q., Song, L.L., Zhou, C.Y., 2015. A comparative study of field measurements of the turbulence characteristics of typhoon and hurricane winds. *J. Wind Eng. Ind. Aerod.* 140, 49–66.
- Li, Q.S., Dai, Y.M., Li, Z.N., Hu, S.Y., 2010. Surface layer wind field characteristics during a severe typhoon "Hagupit" landfalling. *J. Build. Struct.* 31 (4), 54–61 (In Chinese).
- Liepmann, H.W., 1952. On the application of statistical concepts to the buffeting problem. *J. Aeronaut. Sci.* 19 (12), 793–800.
- Lin, Y.K., Li, Q.C., 1993. New stochastic theory for bridge stability in turbulent flow. *J. Eng. Mech.* 119 (1), 113–127.
- Liu, P., Zhao, L., Fang, G.S., Ge, Y.J., 2021. Explicit polynomial regression models of wind characteristics and structural effects on a long-span bridge utilizing onsite monitoring data. *Struct. Control Health Monit.* 28 (5), e2705.
- Øiseth, O., Rønquist, A., Sigbjørnsson, R., 2010. Simplified prediction of wind-induced response and stability limit of slender long-span suspension bridges, based on modified quasi-steady theory: a case study. *J. Wind Eng. Ind. Aerod.* 98 (12), 730–741.
- Scanlan, R.H., Bélineau, J.G., Budlong, K.S., 1974. Indicial aerodynamic functions for bridge decks. *J. Eng. Mech. Div.* 100 (4), 657–672.
- Sears, W.R., 1941. Some aspects of non-stationary airfoil theory and its practical application. *J. Aeronaut. Sci.* 8 (3), 104–108.
- Seo, D.W., Caracoglia, L., 2012. Statistical buffeting response of flexible bridges influenced by errors in aeroelastic loading estimation. *J. Wind Eng. Ind. Aerod.* 104, 129–140.
- Tamura, Y., Shimada, K., Hibi, K., 1993. Wind response of a tower (typhoon observation at the nagasaki huis ten bosch domtoren). *J. Wind Eng. Ind. Aerod.* 50, 309–318.
- Tao, T.Y., Xu, Y.L., Huang, Z.F., Zhan, S., Wang, H., 2020. Buffeting analysis of long-span bridges under typhoon winds with time-varying spectra and coherences. *J. Struct. Eng.* 146 (12), 04020255.
- Von Karman T., 1948. Progress in the statistical theory of turbulence. *Proc. Natl. Acad. Sci. USA* 34 (11), 530–539.
- Wang, H., Li, A.Q., Guo, T., Xie, J., 2009. Field measurement on wind characteristic and buffeting response of the Runyang Suspension Bridge during typhoon Matsa. *Sci. China E* 52 (5), 1354–1362.
- Xu, Y.L., Hu, L., Kareem, A., 2014. Conditional simulation of nonstationary fluctuating wind speeds for long-span bridges. *J. Eng. Mech.* 140 (1), 61–73.
- Yi, G.X., Pan, J.J., Zhao, L., Song, L.L., Fang, G.S., Cui, W., Ge, Y.J., 2022. Profiles of mean wind and turbulence intensity during strong typhoon landfall. *J. Wind Eng. Ind. Aerod.* 228, 105106.
- Zhang, L.T., Cui, W., Zhao, L., Ge, Y.J., 2023. State augmentation method for buffeting responses of wind-sensitive structures in wind environments with large turbulence intensity. *J. Wind Eng. Ind. Aerod.* 240, 105498.
- Zhao, L., Cui, W., Ge, Y.J., 2019. Measurement, modeling and simulation of wind turbulence in typhoon outer region. *J. Wind Eng. Ind. Aerod.* 195, 104021.
- Zhao, L., Xie, X., Zhan, Y.Y., Cui, W., Ge, Y.J., Xia, Z.C., Xu, S.Q., Zeng, M., 2020. A novel forced motion apparatus with potential applications in structural engineering. *J. Zhejiang Univ. - Sci.* 21 (7), 593–608.
- Zhu, L.D., Yan, L., 2015. Wind characteristics of grid-generated wind field along the wind tunnel. *Journal of Experiments in Fluid Mechanics* 29 (1), 49–54 (In Chinese).